

Fall 12-31-2018

Interactions between polymer nanoparticles and blood plasma applied to drug delivery systems

Mark Bannon
New Jersey Institute of Technology

Follow this and additional works at: <https://digitalcommons.njit.edu/theses>



Part of the [Chemical Engineering Commons](#)

Recommended Citation

Bannon, Mark, "Interactions between polymer nanoparticles and blood plasma applied to drug delivery systems" (2018). *Theses*. 1632.

<https://digitalcommons.njit.edu/theses/1632>

This Thesis is brought to you for free and open access by the Electronic Theses and Dissertations at Digital Commons @ NJIT. It has been accepted for inclusion in Theses by an authorized administrator of Digital Commons @ NJIT. For more information, please contact digitalcommons@njit.edu.

Copyright Warning & Restrictions

The copyright law of the United States (Title 17, United States Code) governs the making of photocopies or other reproductions of copyrighted material.

Under certain conditions specified in the law, libraries and archives are authorized to furnish a photocopy or other reproduction. One of these specified conditions is that the photocopy or reproduction is not to be “used for any purpose other than private study, scholarship, or research.” If a user makes a request for, or later uses, a photocopy or reproduction for purposes in excess of “fair use” that user may be liable for copyright infringement,

This institution reserves the right to refuse to accept a copying order if, in its judgment, fulfillment of the order would involve violation of copyright law.

Please Note: The author retains the copyright while the New Jersey Institute of Technology reserves the right to distribute this thesis or dissertation

Printing note: If you do not wish to print this page, then select “Pages from: first page # to: last page #” on the print dialog screen

The Van Houten library has removed some of the personal information and all signatures from the approval page and biographical sketches of theses and dissertations in order to protect the identity of NJIT graduates and faculty.

ABSTRACT

INTERACTIONS BETWEEN POLYMER NANOPARTICLES AND BLOOD PLASMA APPLIED TO DRUG DELIVERY SYSTEMS

**by
Mark Stephen Bannon**

Targeted nanoparticle drug delivery has the potential to replace current forms of cancer therapy with previously unparalleled efficiency. Upon introduction into the human body, nanoparticles exhibit a substantial increase in diameter due to a biomolecular corona formation caused by interactions between blood plasma proteins and the nanoparticles. These interactions must be analyzed and understood for targeted delivery to reach its potential in both feasibility and efficiency.

To study the formation of the protein corona, polystyrene nanoparticles were incubated *in vitro* in goat blood plasma for 10-minute intervals, diluted to different degrees and then measured to obtain the hydrodynamic diameter of said particles. This was done using Nanoparticle Tracking Analysis (NTA) with the Malvern Nanosight NS300's more reliable fluorescent capabilities as opposed to the more commonly used Dynamic Light Scattering Particle Size Analysis (DLS).

The results of this experiment showed that the size of the nanoparticles being incubated in blood plasma increases as the solutions become more dilute. These results were then plotted and characterized by linear regression in order to distinguish between the hard and soft coronas. The experiment also proved that NTA is a more reliable method for measuring nanoparticles in blood plasma than the commonly used DLS. These findings have major implications towards targeted nanoparticle drug delivery and will ultimately contribute to further research in the subject.

**INTERACTIONS BETWEEN POLYMER NANOPARTICLES AND
BLOOD PLASMA APPLIED TO DRUG DELIVERY SYSTEMS**

**by
Mark Stephen Bannon**

**A Thesis
Submitted to the Faculty of
New Jersey Institute of Technology
in Partial Fulfillment of the Requirements for the Degree of
Master of Science in Chemical Engineering**

**Otto H. York Department of
Chemical and Materials Engineering**

December 2018

Blank Page

APPROVAL PAGE

**POLYMER NANOPARTICLE INTERACTIONS WITH BLOOD
PLASMA APPLIED TO DRUG DELIVERY SYSTEMS**

Mark Stephen Bannon

Dr. Kathleen McEnnis, Dissertation Advisor Date
Assistant Professor of Chemical and Materials Engineering, NJIT

Dr. Piero Armenante, Committee Member Date
Distinguished Professor of Chemical and Materials Engineering, NJIT

Dr. Angelo Perna, Committee Member Date
Professor of Chemical Engineering, NJIT

BIOGRAPHICAL SKETCH

Author: Mark Stephen Bannon

Degree: Master of Science

Date: January 2019

Undergraduate and Graduate Education:

- Bachelor of Science in Chemical Engineering,
New Jersey Institute of Technology, Newark, New Jersey, 2018

Major: Chemical Engineering

Dedicated to
My Parents, Mark and Jacquie
and
My Brother, Sean,
Who have made me everything that I am today.

“So be sure when you step, step with care and great tact. And remember that life’s
A Great Balancing Act. And will you succeed? Yes! You will, indeed!
(8 and $\frac{3}{4}$ percent guaranteed) Kid, you’ll move mountains.”

-Theodore Seuss Geisel-

ACKNOWLEDGMENT

Dr. Kathleen McEnnis, Dr. Piero Armenante, Dr. Angelo Perna, Dr. Michel Boufadel,
Leanord Kaplan, Barry Broxton, Sandra Taylor, Aida Lopez, Miriam Marquez,
Karen Reyes, Kourtney Gans, Mohammad Savarmand, Alison Shweh, Sean Bannon,
Judy Young, Mark & Jacquie Bannon

TABLE OF CONTENTS

Chapter	Page
1 INTRODUCTION.....	1
1.1 Objective.....	1
1.2 Background Information.....	1
2 METHOD COMPARISON FOR NANOPARTICLE SIZE MEASUREMENT.....	8
2.1 Dynamic Light Scattering.....	8
2.2 Nanoparticle Tracking Analysis.....	10
2.3 Methods and Materials.....	11
2.4 Results.....	15
3 PLASMA DILUTION EXPERIMENT.....	28
3.1 Methods and Materials.....	28
3.2 Measured Size of Nanoparticles in Blood Plasma.....	29
4 STATISTICAL ANALYSIS OF POLYSTYRENE NANOPARTICLE SIZE DATA.....	31
4.1 Analysis of Variance.....	31
4.2 ANOVA Test on Dilutions of Pure Saline.....	32
4.3 ANOVA Test Across Dilutions of Plasma Batches.....	33
4.4 ANOVA Test Across Separate Plasma Batches.....	36
5 AVERAGE PROTEIN CORONA THICKNESS ANALYSIS.....	37
5.1 Average Thickness of Developed Protein Coronas.....	37
5.2 ANOVA Tests on Average Protein Corona Thickness.....	39

TABLE OF CONTENTS
(Continued)

Chapter	Page
5.3 Statistical Analysis of Average Protein Corona Thickness Regression..	42
6 FUTURE WORK.....	47
6.1 Dilution Experiment Expansion.....	47
6.2 Determining Protein Corona Composition.....	49
6.3 Binding Affinity.....	51
7 CONCLUSION.....	52
APPENDIX A DYNAMIC LIGHT SCATTERING.....	54
A.1 Malvern Zetasizer Nano ZS.....	54
A.2 Dilution Experiment.....	55
APPENDIX B VISCOMETRY.....	72
APPENDIX C Nanoparticle Tracking Analysis.....	76
C.1 Malvern Nanosight NS300.....	76
C.2 Dilution Experiment.....	77
REFERENCES.....	84

LIST OF TABLES

Table	Page
2.1 Amount of Plasma in Numbered Dilutions.....	13
4.1 Single Factor ANOVA Summary of Hydrodynamic Diameters of Nanoparticles Incubated in 10 Incremental Dilutions of Saline.....	32
4.2 Single Factor ANOVA Summary of Hydrodynamic Diameters of Nanoparticles Incubated in 7 Incremental Dilutions of Plasma 1.....	34
4.3 Single Factor ANOVA Summary of Hydrodynamic Diameters of Nanoparticles Incubated in 10 Incremental Dilutions of Plasma 2.....	35
4.4 Single Factor ANOVA Summary of Hydrodynamic Diameters of Nanoparticles Incubated in Plasma 1 and Plasma 2.....	36
5.1 Fitted Equations Developed from the Linear Regression of the Data Plotted in Figure 5.1.....	39
5.2 Single Factor ANOVA Summary of Average Protein Corona Thickness of Nanoparticles Incubated in 7 Incremental Dilutions of Plasma 1.....	40
5.3 Single Factor ANOVA Summary of Average Protein Corona Thickness of Nanoparticles Incubated in 10 Incremental Dilutions of Plasma 2.....	41
5.4 Single Factor ANOVA Summary of Average Protein Corona Thickness of Nanoparticles Incubated in Plasma 1 and Plasma 2.....	42
5.5 Regression Analysis of Fitted Equations Developed from the Data Plotted in Figure 5.1.....	45
A.1 Hydrodynamic Diameters of Polystyrene Particles Incubated in Plasma 2 Using DLS.....	71
B.1 Kinematic Viscosity of Dilutions of Goat Blood Plasma and Saline Solution Converted to Dynamic Viscosity Using Density.....	73
B.2 Actual Density Values of Each Dilution.....	74
C.1 Hydrodynamic Diameters of Polystyrene Nanoparticles Incubated in Plasma 2.....	77

LIST OF TABLES
(Continued)

Table	Page
C.2 Raw Data Used to Calculate the Hydrodynamic Diameters of Polystyrene Nanoparticles Incubated in Plasma 2	78
C.3 Hydrodynamic Diameters of Polystyrene Particles Incubated in Plasma 1.....	79
C.4 Hydrodynamic Diameters of Polystyrene Particles Incubated in Saline Solution.....	80
C.5 Raw Data Used to Calculate the Hydrodynamic Diameters of Polystyrene Particles in Saline Solution.....	81
C.6 Fitted Equations Relating Particle Hydrodynamic Diameter with Percentage of Plasma in Dilution.....	81
C.7 Average Protein Corona Thickness of Polystyrene Particles Incubated in Plasma 1.....	82
C.8 Average Protein Corona Thickness of Polystyrene Particles Incubated in Plasma 2.....	83

LIST OF FIGURES

Figure	Page
1.1 Drug Delivery Nanoparticle Diagram.....	2
1.2 Development of a Protein Corona onto a Nanoparticle.....	4
1.3 Comparison Between Human and Goat Blood Plasma Using Zone Electrophoresis.....	6
2.1 Stokes-Einstein Equation.....	8
2.2 Plotted Hydrodynamic Diameters of Polystyrene Nanoparticles After Incubation in Various Dilutions of Blood Plasma and Saline Solution...	16
2.3 Intensity Plotted Against Size Data Calculated by DLS in the Malvern Zetasizer Nano ZS Assessed According to the Goodness of Fit Shown by the Expert Advice Tab for Saline, Dilution 0.....	17
2.4 Nanoparticle Concentration Plotted Against Size Data Calculated by NTA in the Nanosight NS300 for Saline, Dilution 0.....	18
2.5 Intensity Plotted Against Size Data Calculated by DLS in the Malvern Zetasizer Nano ZS Assessed According to the Goodness of Fit Shown by the Expert Advice Tab for Plasma, Dilution 8.....	20
2.6 Nanoparticle Concentration Plotted Against Size Data Calculated by NTA in the Nanosight NS300 for Plasma, Dilution 8.....	21
2.7 Intensity Plotted Against Size Data Calculated by DLS in the Malvern Zetasizer Nano ZS Assessed According to the Goodness of Fit Shown by the Expert Advice Tab for Plasma, Dilution 6.....	22
2.8 Nanoparticle Concentration Plotted Against Size Data Calculated by NTA in the Nanosight NS300 for Plasma, Dilution 8.....	23
2.9 Diagram of Nanoparticles in Blood Plasma.....	25
2.10 Fluorescently Tagged Nanoparticles in Plasma Viewed through Fluorescent Filter.....	26
3.1 Plotted Hydrodynamic Diameters of Polystyrene Nanoparticles After Incubation in Various Dilutions of Blood Plasma and Saline Solution...	29

LIST OF FIGURES
(Continued)

Figure	Page
5.1 Average Thickness of Protein Corona After Incubation in Various Dilutions of Plasma and Saline Solution for Plasma 1 and Plasma 2....	38
5.2 Minitab Results from a Coefficient Comparison Between Two Independently Developed Coefficients Using a Hypothesis Test.....	44
6.1 Comparison Between Human and Ox Blood Plasma Using Zone Electrophoresis.....	48
A.1 Schematic of Malvern Zetasizer Nano NS.....	54
A.2 DLS Results from Polystyrene Nanoparticles Incubated in Saline, Run #1.....	55
A.3 Description of Data Quality for Saline, Run #1.....	56
A.4 DLS Results from Polystyrene Nanoparticles Incubated in Saline, Run #2.....	56
A.5 Description of Data Quality for Saline, Run #2.....	57
A.6 DLS Results from Polystyrene Nanoparticles Incubated in Saline, Run #3.....	57
A.7 Description of Data Quality for Saline, Run #3.....	58
A.8 DLS Results from Polystyrene Nanoparticles Incubated in Dilution 9, Run #1.....	58
A.9 Description of Data Quality for Dilution 9, Run #1.....	59
A.10 DLS Results from Polystyrene Nanoparticles Incubated in Dilution 9, Run #2.....	59
A.11 Description of Data Quality for Dilution 9, Run #2.....	60
A.12 DLS Results from Polystyrene Nanoparticles Incubated in Dilution 9, Run #3.....	60

LIST OF FIGURES
(Continued)

Figure	Page
A.13 Description of Data Quality for Dilution 9, Run #3.....	61
A.14 DLS Results from Polystyrene Nanoparticles Incubated in Dilution 8, Run #1.....	61
A.15 Description of Data Quality for Dilution 8, Run #1.....	62
A.16 DLS Results from Polystyrene Nanoparticles Incubated in Dilution 8, Run #2.....	62
A.17 Description of Data Quality for Dilution 8, Run #2.....	63
A.18 DLS Results from Polystyrene Nanoparticles Incubated in Dilution 8, Run #3.....	63
A.19 Description of Data Quality for Dilution 8, Run #3.....	64
A.20 DLS Results from Polystyrene Nanoparticles Incubated in Dilution 7, Run #1.....	64
A.21 Description of Data Quality for Dilution 7, Run #1.....	65
A.22 DLS Results from Polystyrene Nanoparticles Incubated in Dilution 7, Run #2.....	65
A.23 Description of Data Quality for Dilution 7, Run #2.....	66
A.24 DLS Results from Polystyrene Nanoparticles Incubated in Dilution 7, Run #3.....	66
A.25 Description of Data Quality for Dilution 7, Run #3.....	67
A.26 DLS Results from Polystyrene Nanoparticles Incubated in Dilution 6, Run #1.....	67
A.27 Description of Data Quality for Dilution 6, Run #1.....	68
A.28 DLS Results from Polystyrene Nanoparticles Incubated in Dilution 6, Run #2.....	68

LIST OF FIGURES
(Continued)

Figure	Page
A.29 Description of Data Quality for Dilution 6, Run #2.....	69
A.30 DLS Results from Polystyrene Nanoparticles Incubated in Dilution 6, Run #3.....	69
A.31 Description of Data Quality for Dilution 6, Run #3.....	70
C.1 Schematic of Malvern Nanosight NS300.....	76

CHAPTER 1

INTRODUCTION

1.1 Objective

This dissertation's objective is to quantify the interactions between drug delivery particles and the biological milieu in which they are working in, in this case blood plasma. For the dilution experiment used, nanoparticles were incubated in different goat blood plasma solutions and then diluted with saline. Said plasma was diluted incrementally for each iteration. Analysis of incubated particle size was done using the Malvern Nanosight NS300, based upon a comparison of results attained using both nanoparticle tracking analysis of the Malvern Nanosight NS300 and dynamic light scattering of the Malvern Zetasizer Nano ZS. The results of said dilution experiment were plotted against the logarithm of the percentage of plasma in each dilution and regressed linearly using Minitab. Statistical analysis was then completed on both the plotted data and the linearly regressed equations to determine the statistical significance of said data.

1.2 Background Information

Nanoparticle drug delivery systems provide a straight-lined method of delivering necessary therapy to parts of the body that require it. This technology has the potential to replace harmful techniques, such as systemic chemotherapy, to treat cancer patients, as it would provide a less harmful and more effective cancer treatment than current techniques can offer. An example of a nanoparticle used for drug delivery within the human body can be found in Figure 1.1.

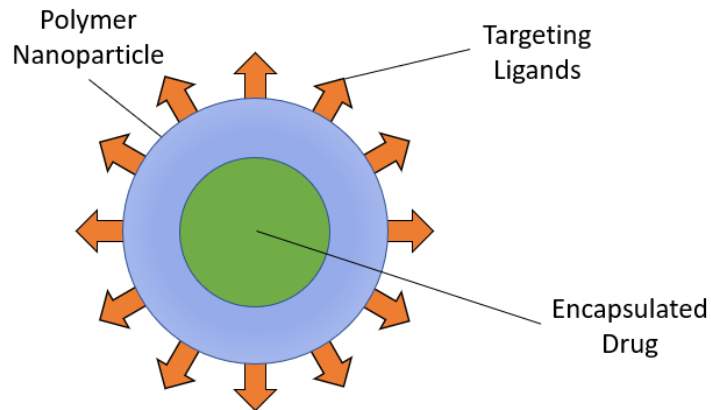


Figure 1.1 Drug Delivery Nanoparticle Diagram

The blue shell of the nanoparticle represents the actual material comprising the nanoparticle, in the specific case described in this paper it would be a polymer such as Polystyrene or PLGA. Other options for this material for drug delivery use include gold or lipid nanoparticles. The green circle within the nanoparticle represents the encapsulated drug meant to be delivered to specific targeted areas within the body. Finally, the orange arrows represent targeting ligands on the surface of the nanoparticles. These ligands can locate and bond to parts of the body in need of the encapsulated drug, such as tumors. This binding allows for the nanoparticle to release its encapsulated drug to the intended parts of the body, completing the drug delivery.

Despite the untapped potential of these systems, there are issues standing between the design and implementation of nanoparticle drug delivery. One of these issues is the interactions that occur between nanoparticles and the blood of the patient receiving therapy. Upon incubation, these nanoparticles demonstrate an affinity to certain compounds that are present in the blood plasma, specifically plasma proteins. This affinity results in a coating

of these blood plasma compounds surrounding the nanoparticles, which can cause either a simple size increase or a large aggregation of particles moving through the body [13].

Upon a nanoparticle's entrance into the bloodstream, one will observe an increase in the particle's hydrodynamic diameter. As the nanoparticle encounters proteins located in the blood plasma, attractions form between the nanoparticle's surface and the proteins, causing the proteins to bind onto the nanoparticle. Unfortunately, these coronas are extremely complex, resulting from possible interactions with the thousands of different proteins at differing concentrations present in the blood. In turn, the protein corona of nanoparticles can differ from patient to patient, incubation to incubation within the same patient and even from nanoparticle to nanoparticle during the same incubation.

The protein corona can be separated into two different phases: the hard corona and the soft corona. The current model of a protein corona shows that the hard corona is comprised of proteins that are directly bound to the nanoparticle surface, acting as an outer shell around the particle itself [13]. The main method of this protein adsorption is entropy-driven binding, which occurs upon the release of water molecules from the surface of the nanoparticle. The second part of the corona, the soft corona, comprises of proteins that loosely bind to either the nanoparticle's surface or the hard corona proteins themselves, creating protein-protein interactions [13]. The overall development of a protein corona onto a nanoparticle can be demonstrated by Figure 1.2.

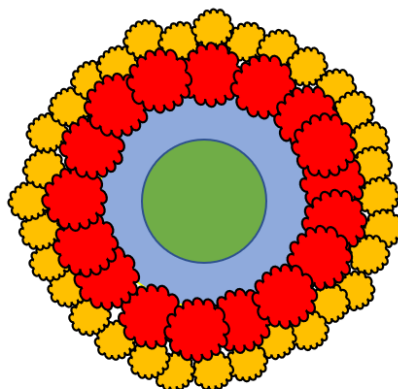


Figure 1.2 Development of a Protein Corona onto a Nanoparticle

Figure 1.2 represents a protein corona formed upon incubation of one of the nanoparticles described by Figure 1.1. The red and yellow shapes represent different proteins contributing to the hard and soft corona; however, it is important to remember that both layers can be made of a mixture of different proteins. Figure 1.2 shows that the orange targeting ligands are no longer visible on the surface of the particle. The soft protein corona primarily contributes to the corona's overall masking effect, which chemically changes the composition of the particle within its incubated biological milieu. This masking effect blocks the targeting ligands from locating and binding to locations in the body that require the drug encapsulated within the nanoparticle [19]. This diagram shows the negative effects of protein corona, which can lead to the failure of drug delivery systems.

The composition of the protein corona is determined from many variables, which include (but are not limited to) nanoparticle size, shape, composition, surface charge, hydrophobicity/hydrophilicity, etc. Another very important variable affecting the size and composition of the protein corona is the surface chemistry of the nanoparticle. There are many methods to change a nanoparticle's surface chemistry, however one of the most

effective methods is through PEGylation. PEGylation refers to adding polyethylene glycol chains to the surface of the nanoparticles, which makes the particle much more hydrophilic and therefore less prone to aggregation and large protein coronas [13].

While the variables previously discussed contribute heavily to the formation of protein coronas on select nanoparticles, the corona composition during incubation is governed by a law known as Vroman's effect. This law states that the most abundant proteins are adsorbed onto the nanoparticle surface upon initial incubation, however as time goes on proteins with higher affinity to the nanoparticles will replace the initially adsorbed proteins [13]. This presents an even bigger issue, as it Vroman's effect dictates that the protein corona is changing over time, with new proteins constantly adsorbing onto and desorbing from the surface of the nanoparticle. However, it does let us know that proteins such as albumin, fibrinogen, apolipoproteins and certain immunoglobulins (among the most abundant proteins in the blood plasma) should always be present on the protein corona in some capacity [19].

While Vroman's effect is hard enough to predict, the nanoparticles being incubated in blood plasma will constantly be in motion, which the conducted experiments do not account for. When nanoparticles are incubated in a dynamic environment, the effect of Brownian motion must be considered. Brownian motion is based upon random movement of particles in suspension, which causes the nanoparticle surface adsorption of a plasma protein to be dependent upon the probability of that specific protein species to encounter the nanoparticle. By this logic, larger proteins and proteins in high abundance are more likely to adsorb onto the nanoparticles and become part of the protein corona, as they take

up a larger volume within the bloodstream and are more likely to collide with the nanoparticles [13]. Brownian motion will be discussed in greater detail in Chapter 2

The masking effect that accompanies these interactions between the nanoparticles and blood plasma components ultimately causes drug delivery through these nanoparticle systems to become a near impossible task. In order to efficiently implement nanoparticle drug delivery to its full potential, one must first understand the interactions between the nanoparticles and the plasma components. For this reason, it is extremely important to understand not only how Vroman's effect collaborates with Brownian motion, but also how to control the two laws.

The plasma being used for this experiment is derived from goat blood. While the eventual drug delivery systems will be applied to human test subjects, goat plasma serves as an effective and safer substitute. A study done by Morris et al compared human blood plasma with that of various animals, including goats, by zone electrophoresis.

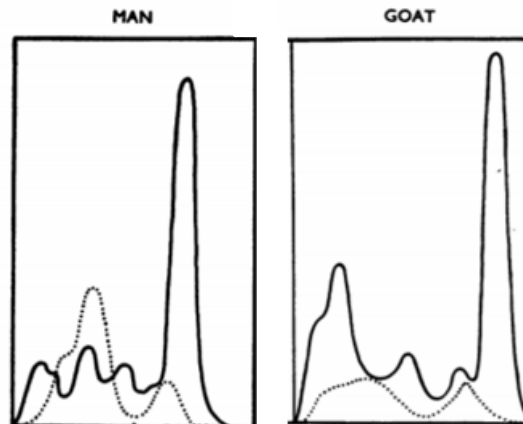


Figure 1.3 Comparison between Human and Goat Blood Plasma Using Zone Electrophoresis

Source: Morris, Bede, and F. C. Courtice. "The Protein And Lipid Composition Of The Plasma Of Different Animal Species Determined By Zone Electrophoresis And Chemical Analysis." *Quarterly Journal of Experimental Physiology and Cognate Medical Sciences*, vol. 40, no. 2, 7 Nov. 1955, pp. 127–137., doi:10.1113/expphysiol.1955.sp001104.

The above graphs display the similarities between goat and human blood plasma. The large peak on the right indicates the relative amount of the plasma protein albumin in both types of blood: the results clearly show that goat blood plasma contains more. Goat blood plasma also contains higher concentrations of gamma globulin and fibrinogen, two proteins very abundant in human blood plasma. Goat blood plasma also contains beta and alpha globulin fractions. The major difference comes with the lipid composition. Zone electrophoresis separated lipids available in human plasma into three distinct categories, while goat blood plasma's lipids were only separated into two categories. Despite this minor difference, Morris confirms that it is acceptable to use goat blood plasma as a substitute for human blood plasma [16].

CHAPTER 2

METHOD COMPARISON FOR NANOPARTICLE SIZE MEASUREMENT

2.1 Dynamic Light Scattering

Dynamic light scattering is the most common technique used to size nanoparticles in suspensions [19]. When in a suspension such as blood plasma, nanoparticle movement adheres to the laws of Brownian motion, which is used to describe the randomized movement of microscopic particles in a fluid. This erratic movement is usually a result of constant bombardment by molecules of the surrounding medium, which in these experiments is blood plasma [6]. Because these particles are so small, and their randomized location makes it impossible to predict their locations, it is quite difficult to see, and therefore size, these particles. DLS transmits waves of light through a suspension with microscopic particles. The particles will scatter this transmitted light, which allows for their state of motion to be measured [10].

DLS uses the Stokes-Einstein equation to calculate a particle's hydrodynamic diameter. The Stokes-Einstein equation can be shown in Figure 2.1:

$$d(H) = \frac{kT}{3\pi\eta D}$$

Figure 2.1 Stokes-Einstein Equation

Source: Wade Hedegard, Anatomy & Physiology: Fluids and Transport. OpenStax CNX. Jun 27, 2017

In the above equation, “ k ” represents Boltzmann’s constant, “ T ” represents absolute temperature, and “ η ” represents the dynamic viscosity of the suspension. DLS measures the parameter “ D ”, which is the translational diffusion coefficient. This parameter describes the speed of the Brownian motion [6]. Because the other parameters are usually known, it becomes easy to measure “ $d(H)$ ”, which represents the hydrodynamic diameter of particles in suspension. Hydrodynamic refers to “how a particle diffuses within a fluid”. Because it is impossible to know the exact shape of the particles through DLS, the hydrodynamic diameter represents the diameter of a sphere that has the same translation diffusion coefficient as the particle [6].

DLS calculates this hydrodynamic diameter using the measured intensity of light scattered from particles in suspension. This intensity is then fit to a correlation curve, where the correctness of fit is determined for the measured data. The correlation curve will always be used to calculate the perceived hydrodynamic diameters of the particles, however the accuracy of said curve depends upon the quality of the data measured from a sample [6].

While dynamic light scattering is a useful technique for nanoparticle sizing, it has a significant drawback that prevents it from being reliable for sizing polymer nanoparticles in blood plasma. Blood plasma has an innumerable amount of proteins in it, which just as readily scatter light as the polymer nanoparticles being used in drug delivery solutions. The problem is that as plasma is introduced into the solution, a large amount of plasma proteins enters the system, which can create variation in the measurements in two ways. One, variation in the sizes of particles present in suspension will affect the correlation curve and produce a less accurate fit of size data. Second, as there becomes a greater concentration of similarly sized proteins (or other blood plasma constituents) than polymer nanoparticles

in the solution, then DLS will be measuring the size of those more abundant proteins. This makes it nearly impossible to measure the size of nanoparticles in solvents mainly comprised of blood plasma. To understand how these particles behave in the blood stream, it is important to be able to measure their size in pure blood plasma. While DLS is a more common and perfected technique for particle sizing, its ambiguity in nanoparticle selectivity provides a problem in implementation.

2.2 Nanoparticle Tracking Analysis

The idea of nanoparticle tracking analysis is similar to that of dynamic light scattering, where a laser is sent through a microfluidic device containing a suspension of particles in blood plasma. It also uses the Stokes-Einstein equation to calculate hydrodynamic diameters of particles. As opposed to DLS, NTA analyzes the individual sizes of nanoparticles by measuring the translational diffusion coefficient of each nanoparticle in suspension. The mode size of particles present in the suspension will then be reported, according to the concentration of the particles in suspension per milliliter [14].

As discussed in the previous section, DLS has trouble differentiating between the proteins found in blood plasma and the nanoparticles in suspension. NTA has the convenience of customized lasers and fluorescent filters, which send out specific wavelengths of light that can excite the fluorescently tagged nanoparticles. The fluorescent light from the fluorescently tagged particles has a higher wavelength than the laser used to excite them; for example, if a 488-nanometer laser was sent into the suspension, the fluorescent light from the fluorescent yellow-green tagged nanoparticles would be over 500 nanometers. On the contrary, particles that aren't fluorescently tagged, such as proteins

found in blood plasma, will only scatter light at the same wavelength of the laser. If a 500 nm fluorescent filter is being used, the scattered light at 488 nm will be blocked and only the fluorescent light from the nanoparticles will be analyzed [14].

Essentially, the fluorescent capabilities of NTA allow users to measure only their targeted particles in suspensions while blocking the scattered light from unwanted particles. This unwanted scattered light is also referred to as “noise”. This enhanced measuring selectivity makes NTA a theoretically superior method of sizing drug delivery nanoparticles in suspensions containing blood plasma. In addition, the fluorescent capabilities of NTA could theoretically allow a user to determine the size of particles in undiluted blood plasma, which is not possible in DLS. The theoretical capabilities of NTA make it a more suitable technique for evaluating polymer drug delivery nanoparticles in blood plasma than DLS [14].

2.3 Methods and Materials

Whole goat blood with Alsevers solution was purchased from Lampire Biological Laboratories. Alsevers solution served as the anticoagulant in the blood and refers to an isotonic salt solution. The specific blood purchased comprised of 50% Alsevers solution and 50% whole goat blood. Whole goat blood with Alsevers solution was chosen to match the same type of blood used in earlier experiments so comparisons could be made between the two samples. The blood was centrifuged for one hour, after which the resulting supernatant was removed and then centrifuged for another hour. This process was repeated three total times until the blood cells were removed and blood plasma was attained.

Plasma accounts for about 55% of whole blood, and therefore after centrifugation the resultant solution is about 35.50% plasma and 64.50% isotonic salt solution, making the highest attainable percentage of plasma in dilution, which is represented by dilution 0, 35.50% [4] [6] [20] [21] [24]. Because of the heavy dilution, the mixture of goat plasma and Alsevers will be referred to as “plasma solution”.

The polystyrene particles were incubated in various amounts of plasma for 10 separate dilutions. Each dilution contains 10 microliters of polystyrene nanoparticle solution (made of 100 microliters of stock yellow-green fluorescently-tagged polystyrene nanoparticle solution diluted with 900 microliters of saline solution) in 1000 microliters of a saline solution and plasma mixture. Dilution 0 contained 1000 microliters of plasma solution, with the amount of plasma in solution incrementally halved until dilution 9, the final dilution, contained 1.95 microliters of plasma solution and 998.05 microliters of saline solution. Table 2.1 summarizes each dilution, describing the amount of plasma and isotonic salt solution (Alsevers and saline) in each solvent dilution. The percentage of plasma solution in each dilution can be found in the second column of Table 2.1.

Table 2.1 Amount of Plasma in Numbered Dilutions

Dilution #	Volume of Incubation Solution (μL)	Percentage of Plasma in Final Dilution (μL)	Volume of Plasma in Final Dilution (μL)	Volume of Saline in Final Dilution (μL)
Dilution 0	1000.00	35.50%	355.00	645.00
Dilution 1	500.00	17.75%	177.50	822.50
Dilution 2	250.00	8.88%	88.75	911.25
Dilution 3	125.00	4.44%	44.38	955.62
Dilution 4	62.50	2.22%	22.19	977.81
Dilution 5	31.25	1.11%	11.09	988.91
Dilution 6	15.63	0.55%	5.55	994.45
Dilution 7	7.81	0.28%	2.77	997.23
Dilution 8	3.91	0.14%	1.39	998.61
Dilution 9	1.95	0.07%	0.69	999.31

Each particle suspension was vortexed for 10 seconds, and then placed in a water bath at 37°C for 10 minutes, which simulated environmental conditions of the human body. After this 10 minute incubation period, saline was added to the solution until it had a volume of 1000 microliters, or 1 milliliter. The saline solution was previously heated to 37°C for the same amount of time as the particle suspension to ensure that a constant temperature was maintained. For this specific experiment, dilutions 6 through 9 as well as nanoparticles measured in pure saline solution were prepared and analyzed using DLS and NTA. For the solution of pure saline, 10 microliters of polystyrene nanoparticle solution were incubated in 1000 microliters of saline solution at 37°C for 10 minutes.

First, for DLS, the solution was loaded into a disposable plastic cuvette by means of transfer pipette. This plastic cuvette was then loaded into a Malvern Zetasizer Nano ZS, of which a schematic can be found in Figure A.1. A standard operating procedure was created in which 3 sets of 12 measurements were taken to analyze the size of any particles in solution, each measurement lasting 5 seconds. For each set, the results of the 12 measurements were averaged together to determine the most commonly recurring peak sizes, or modes, of the hydrodynamic diameter data analyzed. For each dilution, the peak with the highest intensity, or the most commonly recorded peak size, was taken and averaged together to retrieve one overall dilution peak size. The full summary of analyzed data from the DLS can be found in Table A.1.

In the case of NTA, the respective dilutions were loaded into the Nanosight NS300 and pumped continuously through the microfluidic viewing device. The syringe pump was set to a flow rate of 100, which is measured using an arbitrary unit interpreted by the Nanosight NS300. This flow rate resulted in particles crossing the viewing area in five to ten seconds, the recommended time for particle analysis by NTA. The inner chamber of the Nanosight was then set to 37°C to maintain solution temperature throughout the experiments. This temperature mimics the temperature within the human body, allowing for the system to simulate the environment that the nanoparticles would experience in the body with as much accuracy as possible. The solution was analyzed using a 488-nanometer laser and a 500-nanometer fluorescent filter. A schematic of the Nanosight NS300 can be found in Figure C.1

Sizing was completed by recording 10 one-minute videos of the particles in solution, and then allowing the Nanosight NS300 to analyze said videos. This protocol was

repeated three times for each of the ten dilutions until there were over 20 reliable video analyses. To be considered reliable, each solution had to have a concentration of at least 1×10^8 particles per mL and not exceed minor vibration within the sample run time. If the sample was deemed acceptable, the mode hydrodynamic diameter of every fluorescently tagged particle was then calculated by the Stokes-Einstein equation (see Figure 2.1). The generalized particle size of each particle in solution was then determined by the mode of the calculated diameters from the Nanosight NS300's analyzing capabilities.

Finally, referring to Figure 2.1, the Stokes-Einstein equation takes the dynamic viscosity of the solvent being used into effect. Because each dilution's viscosity is different, kinematic viscosity measurements had to be individually performed on each of the ten dilutions using a glass kinematic viscometer and then converted into dynamic viscosity. This can theoretically be done by multiplying the kinematic viscosity of a solution by the solution's density, which was measured for each dilution used. The viscosity of each separate dilution was measured and taken into account to achieve accurate results, which is further discussed in Appendix B.

2.4 Results

The experiments explained in Section 2.3 resulted in measured hydrodynamic diameters of nanoparticles after incubation in various plasma dilution. This data is summarized in Tables A.1 and C.1 and is also plotted in Figure 2.2.

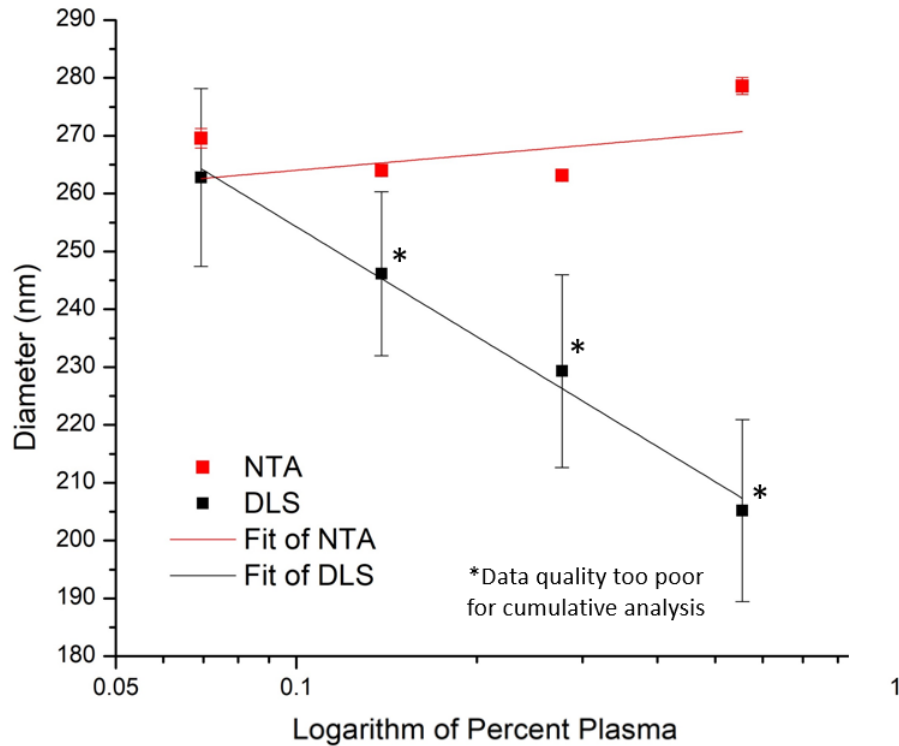


Figure 2.2 Plotted Hydrodynamic Diameters of Polystyrene Nanoparticles After Incubation in Various Dilutions of Blood Plasma and Saline Solution

Figure 2.2 shows the vast differences between the measurements taken by the two systems, where experiments were performed on dilutions 6 through 9. The asterisks next to the data points indicate that data quality used to create said points on the graph was too poor for an accurate result using the correlation function of DLS. Each plotted point represents the average of the mode hydrodynamic particle diameters for each individual measurement in DLS and NTA.

Firstly, the standard error of each measurement using DLS is much greater than that of the NTA NS300. This is made visually apparent by the graph; however, as seen in Tables A.1 and C.1, the error produced by the Nanosight NS300 is in between 1 and 4 nanometers, while the error produced by the DLS is in between 9 and 17 nanometers. The low standard

error boasted by the Nanosight NS300 makes it a superior instrument, and as these experiments deal with extremely small size difference, it would create more reliable results than DLS.

In order to accurately assess the results of these two methods, a comparison of the development of the results must be done. Figures 2.3 and 2.4 show a comparison between the hydrodynamic diameters visually plotted by both DLS and NTA, respectively.

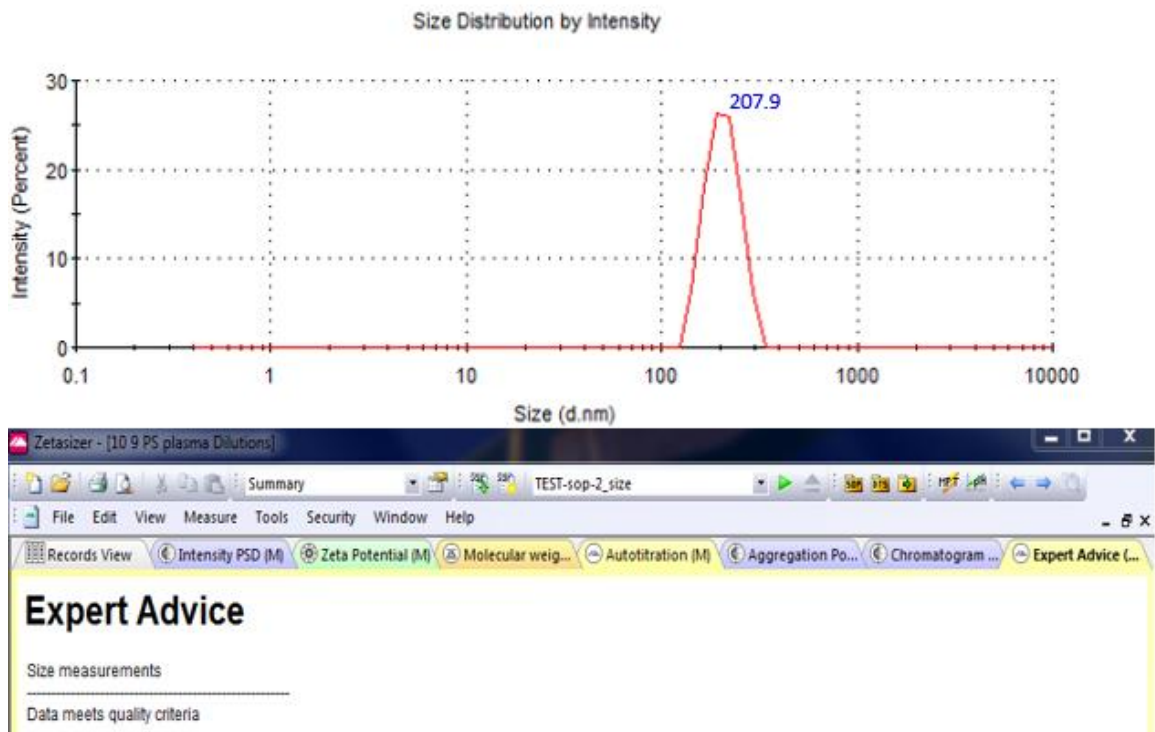


Figure 2.3 Intensity Plotted Against Size Data Calculated by DLS in the Malvern Zetasizer Nano ZS Assessed According to the Goodness of Fit Shown by the Expert Advice Tab for Saline, Dilution 0

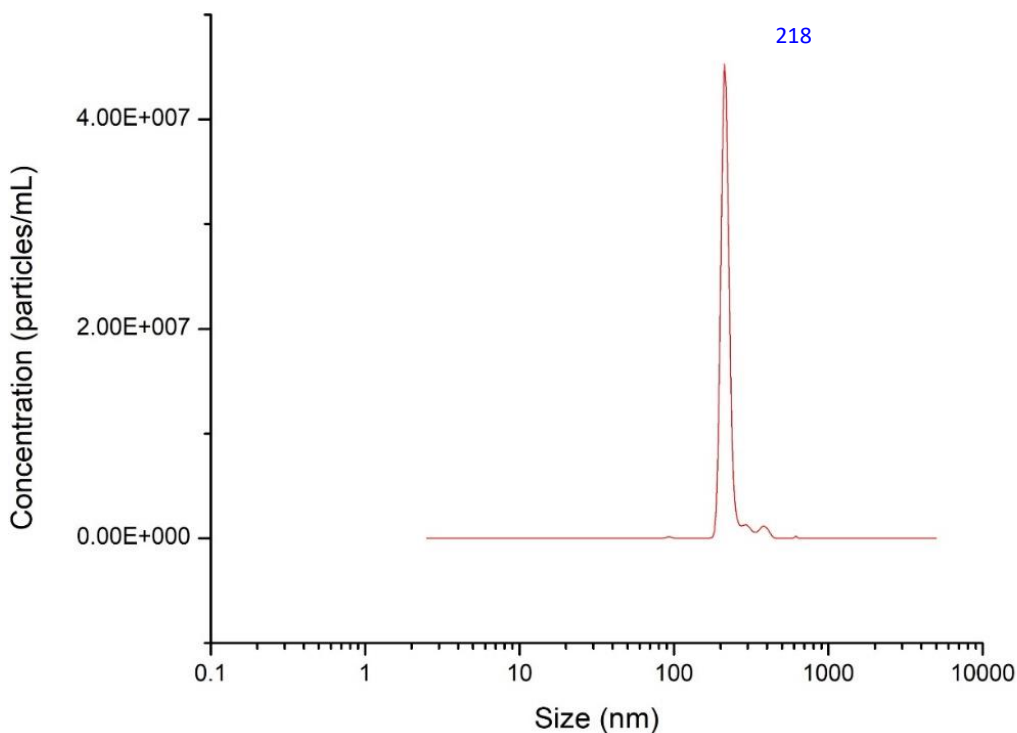


Figure 2.4 Nanoparticle Concentration Plotted Against Size Data Calculated by NTA in the Nanosight NS300 for Saline, Dilution 0

Figure 2.3 shows the results of an individual DLS measurement characterized by the intensity of scattered light from particles in suspension plotted against their sizes on a semi log plot. Figure 2.4 shows the results of an individual NTA measurement characterized by the concentration of particles in suspension, also plotted against their sizes on a semi log plot. Both results are for particles incubated in pure saline.

Clearly, according to the expert advice tab for DLS’s measurement of particles in pure saline, the “data meets quality criteria”, meaning that it is accurate enough to calculate the size of the nanoparticles in suspension correctly. Therefore, the 207.90 nanometer size of the particles can be considered an accurate measurement. This is also comparable to the size of nanoparticles measured by the Nanosight NS300, which is 218.00 nm. Because

these two methods are analyzing size in different ways (NTA by number and DLS by intensity), they are not expected to produce exactly similar hydrodynamic diameters.

Based on these results, both methods measure accurate hydrodynamic diameters of nanoparticles with limited error in a suspension of pure saline; however, the peak width of the Nanosight NS300's data is clearly much smaller than the peak width of the Malvern Nanosight NS300's data. This peak width is another testament to the accuracy of the Nanosight NS300 in saline size measurements, as the thinner peak represents less variable size measurements in each device. This trend of the Nanosight NS300's thinner peaks will continue throughout the dilutions.

Figures 2.5 and 2.6 represent the result of nanoparticle incubation in Dilution 8, which contains a small amount of plasma.

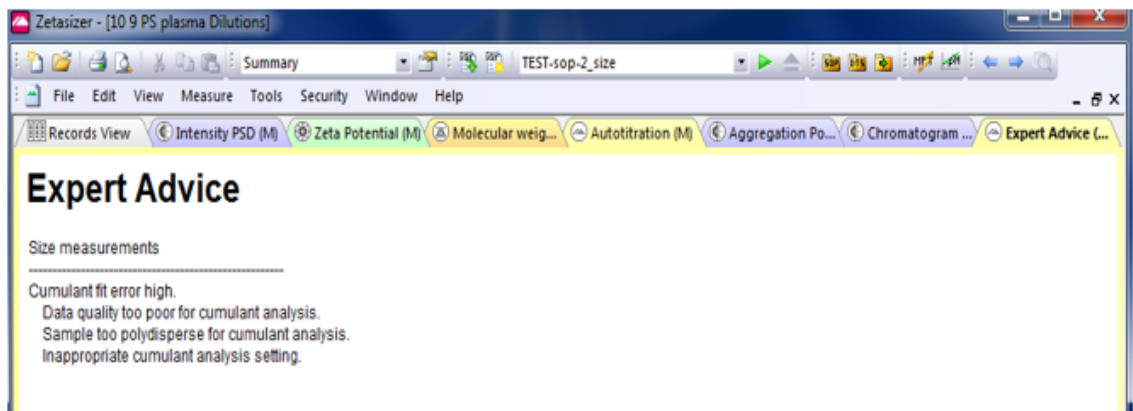
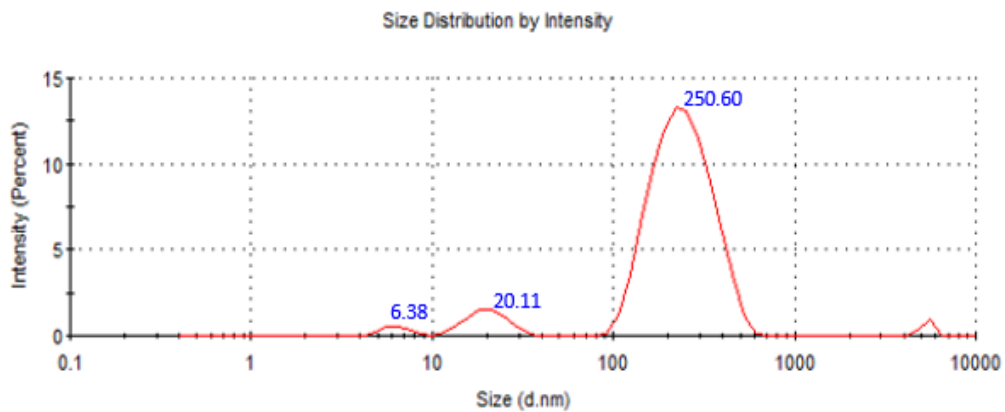


Figure 2.5 Intensity Plotted Against Size Data Calculated by DLS in the Malvern Zetasizer Nano ZS Assessed According to the Goodness of Fit Shown by the Expert Advice Tab for Plasma, Dilution 8

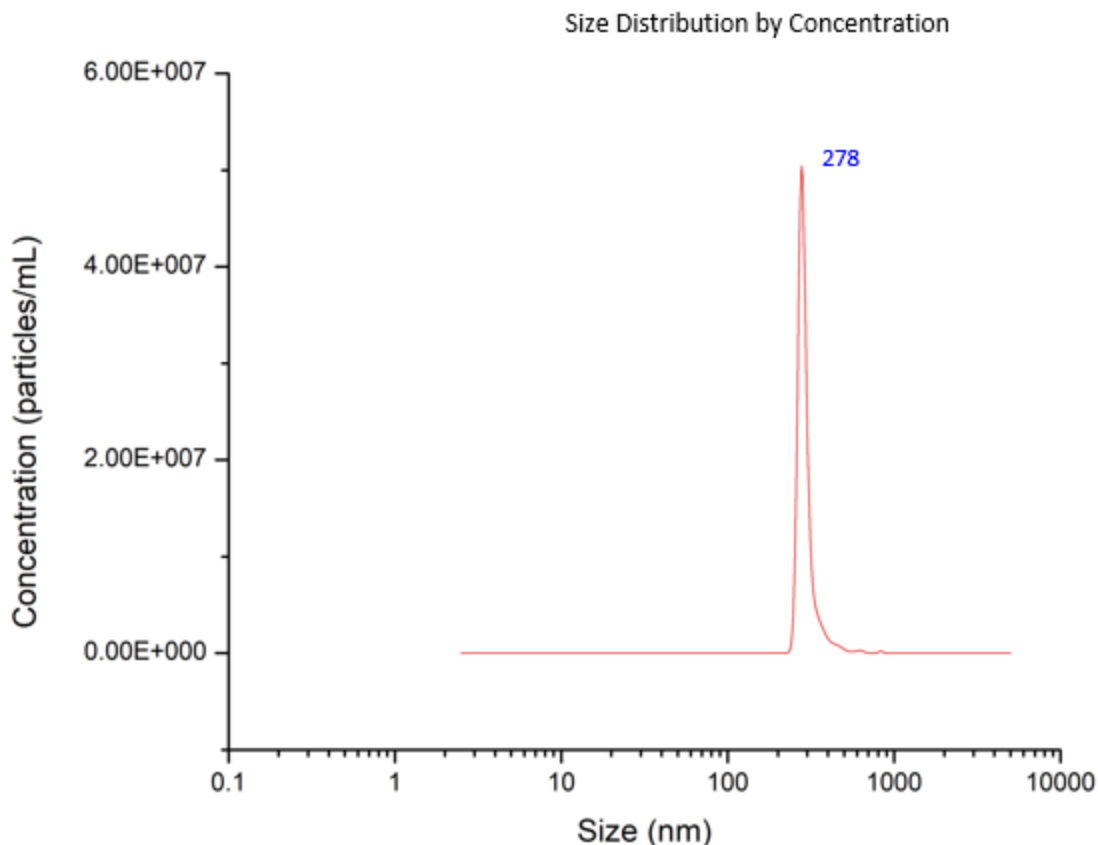


Figure 2.6 Nanoparticle Concentration Plotted Against Size Data Calculated by NTA in the Nanosight NS300 for Plasma, Dilution 8

Once again, Figure 2.5 and 2.6 represent the results of two individual runs of Dilution 8 on the Nanosight NS300 and the Malvern Zetasizer. Unlike Figure 2.3, the Expert Advice reports the data quality as “too poor for cumulant analysis”, meaning that the correlation function used to size the data had too much error to accurately measure the hydrodynamic diameters using DLS. This is because there was too much variation in scattered light within the data, which one can only assume to be resulting from the addition of plasma and its inherent plasma proteins. Because the data quality is considered poor, the measured hydrodynamic diameter of 250.60 cannot be considered an accurate measurement. At the same time two other peaks are present in Figure 2.5, at 6.38 and 20.11

nm. The addition of plasma could lead one to assume that these two peaks represent different components within the plasma, most likely plasma proteins.

The peak of the NTA is still extremely defined, with no other peaks even coming close to the high concentration of the peak representing 278 nm. There is obviously a much larger difference between the results from DLS and NTA, and the poor quality of the DLS correlation fit leads users to consider the NTA's measurement of 278 nm to be more accurate. Once again, the Nanosight NS300's plotted data has a much narrower peak than the Zetasizer ZS's. Obviously, as plasma is added to the incubating solution, there is a decrease in accuracy and reliability in results from DLS. Figures 2.7 and 2.8 show DLS and NTA data, respectively, for Dilution 6.

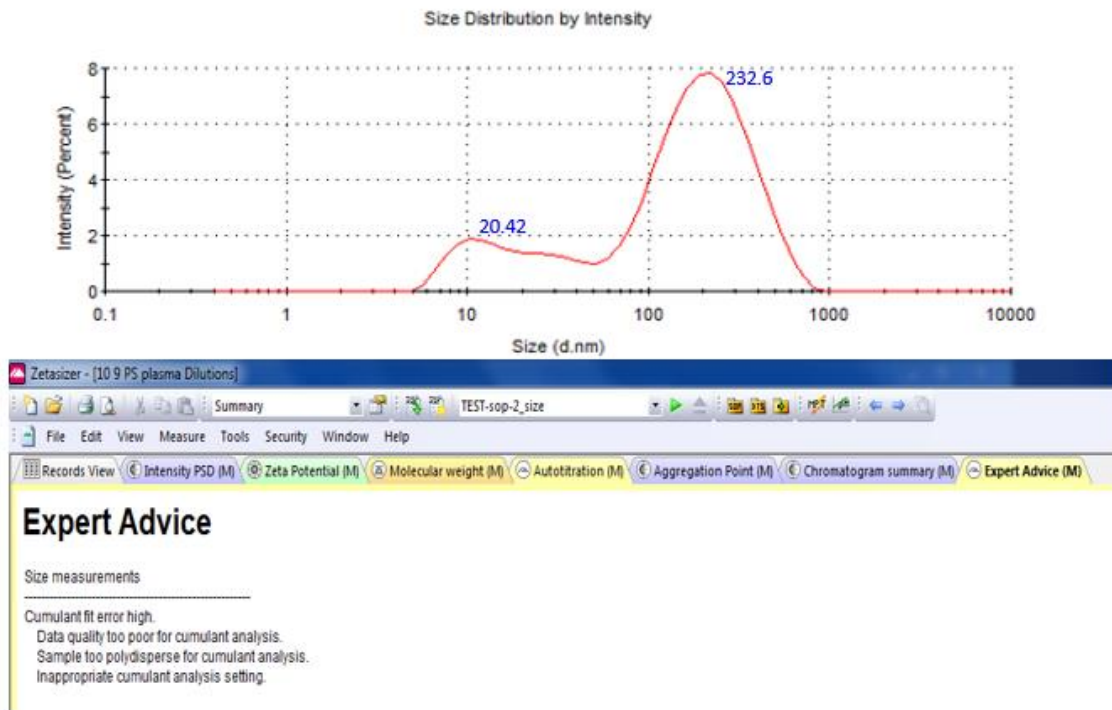


Figure 2.7 Intensity Plotted Against Size Data Calculated by DLS in the Malvern Zetasizer Nano ZS Assessed According to the Goodness of Fit Shown by the Expert Advice Tab for Plasma, Dilution 6

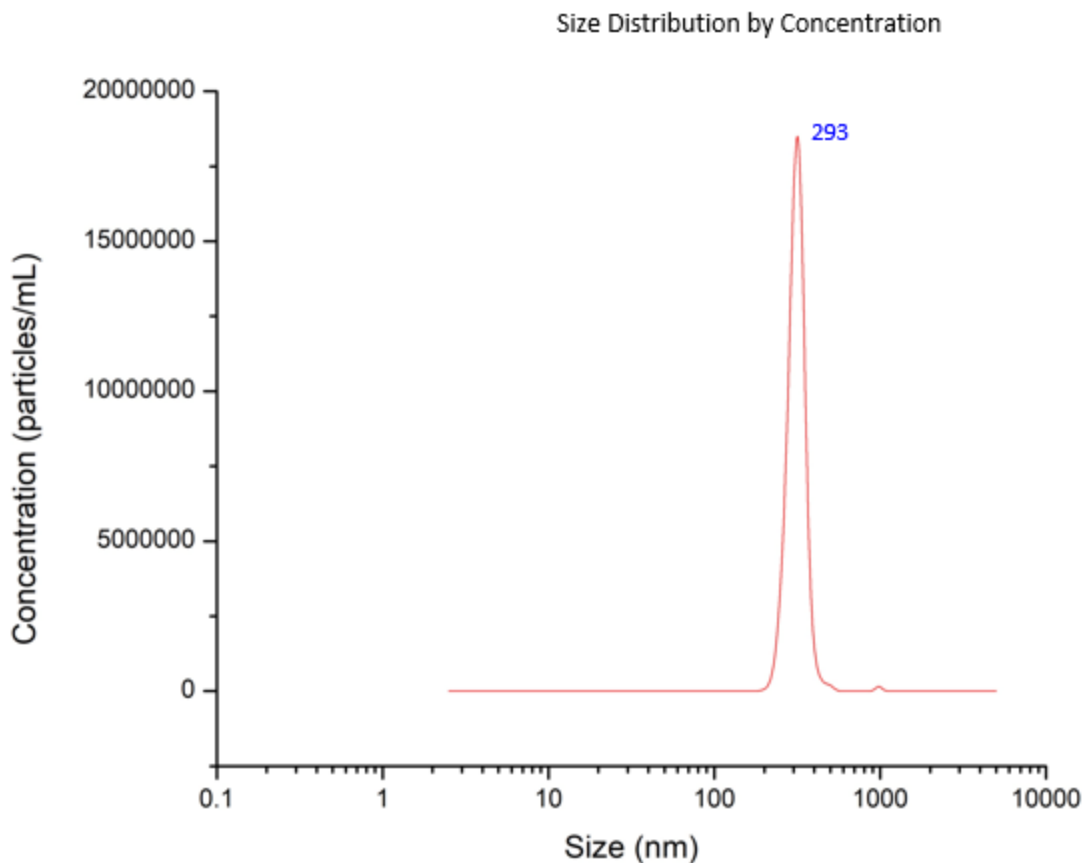


Figure 2.8 Nanoparticle Concentration Plotted Against Size Data calculated by NTA in the Nanosight NS 300 for Plasma, Dilution 6

Once again, Figure 2.7 and 2.8 represent the results of two individual runs of Dilution 6 on the Nanosight NS300 and the Malvern Zetasizer. The Expert Advice reports the data quality as “too poor for cumulant analysis” for Dilution 6, meaning that the correlation function used to size the data had too much error to accurately measure the hydrodynamic diameters using DLS. Because the data quality is considered poor, the measured hydrodynamic diameter of 232.60 nm cannot be considered an accurate measurement. It is also important to note that this size is smaller than that calculated by DLS in Dilution 8, while the size for NTA is conversely increasing as the solutions become

less dilute. It is safe to assume that the fit of the correlation function in the DLS measurement becomes poorer as more plasma is present in incubation and that this trend does not accurately reflect the real trend followed by incubated nanoparticles. The other peaks from Figure 2.5 are present in Figure 2.7 as well, and have increased in intensity, with the peak of 20.11 nm becoming comparable to the peak of 232.60. This also advocates the lower quality of Dilution 6's data as opposed to Dilution 8's in the Zetasizer ZS.

The peak of the NTA is still extremely defined, with no other peaks even coming close to the high concentration of that representing the 293 nm particles. Once again, conversely to DLS data, the size of the nanoparticles is increasing as the dilutions become less dilute. There is obviously a much larger difference between the results from DLS and NTA, and the poor quality of the DLS correlation fit leads users to consider the NTA size of 293 nm more accurate. The Nanosight NS300's plotted data still has a much narrower peak than the Zetasizer ZS's. As the solutions become less dilute, there is a decrease in accuracy and reliability in results from DLS.

Obviously, one of these methods is providing flawed measurements of nanoparticle sizes in blood plasma. In theoretical terms, one would be inclined to claim that DLS presents flawed measurements as the percentage of plasma in dilution increases, which is supported by the poor quality of data used in the correlation function of the Zetasizer ZS's measurements. Figure 2.9 provides an explanation for this poor data quality.

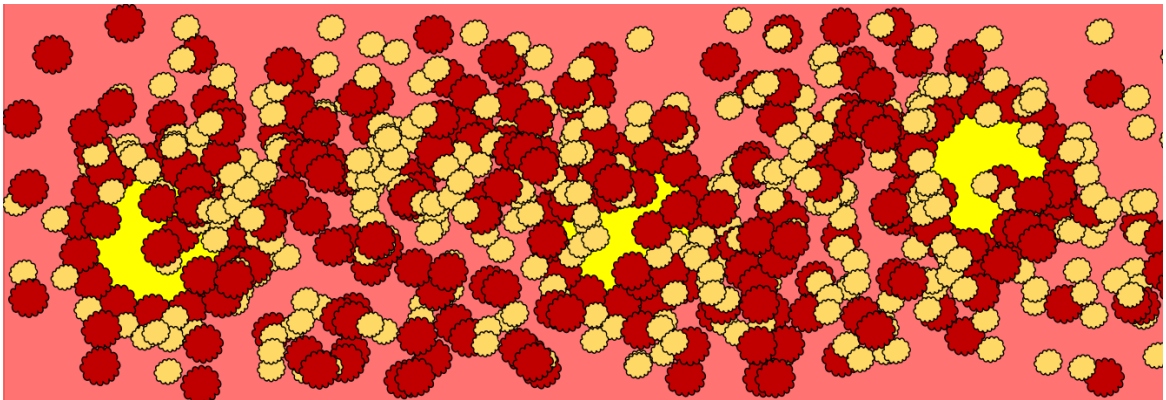


Figure 2.9 Diagram of Nanoparticles in Blood Plasma

Figure 2.9 represents a suspension of fluorescently tagged nanoparticles in blood plasma, much like the ones used in these experiments. The red, translucent background represents the blood plasma while the abundant, small red and yellow circular shapes represent plasma proteins within the plasma. The bright yellow fluorescently tagged polystyrene nanoparticles can still be clearly seen, however it would be impossible to measure the size of these nanoparticles due to the plasma proteins surrounding them. DLS shares this problem. There are thousands of different proteins in blood plasma, meaning that even if the different scattered light did not affect the quality of the data, the scattered light from the plasma proteins would be measured due to the higher concentration of proteins in solution. This can be compared to the fluorescent capabilities of the Nanosight NS300, which can be seen in Figure 2.10.

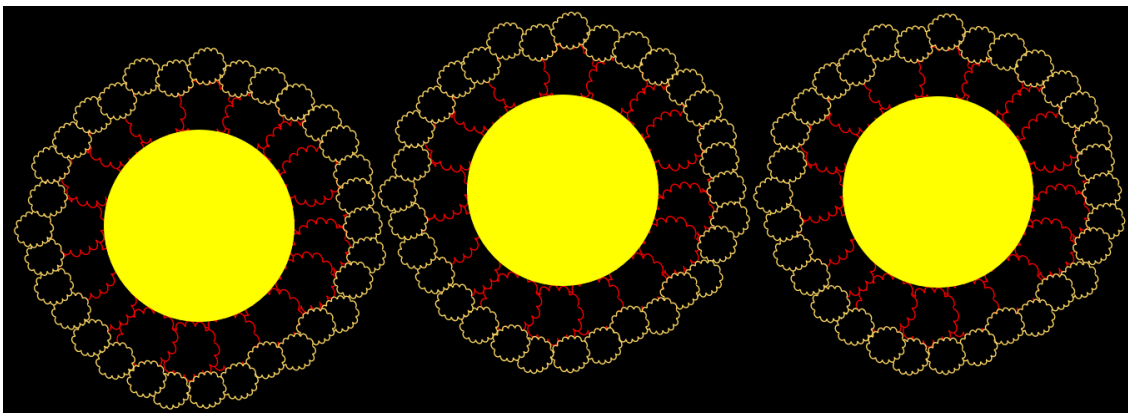


Figure 2.10 Fluorescently Tagged Nanoparticles in Plasma Viewed through Fluorescent Filter

Figure 2.8 shows scattered light from fluorescently tagged nanoparticles viewed on the Nanosight NS300. Using the proper combination of lasers and fluorescent filters, the scattered light from the plasma proteins is not analyzed by the NS300, and only the fluorescent light from the fluorescently tagged nanoparticles is analyzed. Figure 2.10 still shows the outline of the protein corona formed onto the fluorescently tagged nanoparticles. Even though the light scattered by the protein corona is blocked by the filter, it's existence still affects how the nanoparticles move through the suspension and will therefore affect the measured translational diffusion coefficients of the nanoparticles.

The poor data quality displayed in the results is theoretically explained by the abundance of plasma proteins in each solution, which in turn affects the Zetasizer ZS's correlation function, making the results less accurate. The clear and concise peaks shown by the measurements of the Nanosight NS300 can be explained by the use of fluorescent filters, which block all scattered light other than that from the fluorescently tagged polystyrene nanoparticles. After looking at both the theoretical usages and the measured data sets, it is clear that NTA through the Nanosight NS300 is more reliable than DLS through the Malvern Zetasizer Nano ZS for measuring the size of nanoparticles in blood

plasma. For that reason, the Nanosight NS300 was used for the dilution experiments to size polymer nanoparticles in blood plasma.

CHAPTER 3

PLASMA DILUTION EXPERIMENT

3.1 Methods and Materials

As discussed in Chapter 2, the Nanosight NS300 provides the most accurate size measurements of nanoparticles in blood plasma, and therefore was the primary instrument used to do so. Both the solution preparation and the Nanosight NS300 operation were previously described in Section 2.2, and no changes were made to either of those procedures to carry out the experiments discussed in this section. In addition to measuring dilutions 6 through 9, the remaining dilutions were also prepared, measured and analyzed using the Nanosight NS300.

The dilution experiments were carried out on two separate batches of goat blood plasma, both ordered from Lampire Biological Laboratories. One of the experiment sets was carried out in the Spring of 2016 by Dr. Kathleen McEnnis while the second set was carried out in the Summer of 2018 by Mark Bannon. The same exact stock solution of polystyrene nanoparticles was used for each of the sets of experiments. The goat blood plasma batch used in the set of 2018 experiments will be referred to as “Plasma 2”, while the batch used in 2016 will be referred to as “Plasma 1”. To properly analyze the effects of the plasma dilutions and eventual protein corona formation on the incubated polystyrene particles, a control of measured polystyrene particles in pure saline solution was deemed necessary.

A control solution was created for each of the ten dilutions. Just like the plasma dilutions, 10 microliters of polystyrene nanoparticles were incubated using the same exact procedure, however the specific volume of plasma solution used for incubation was

replaced with the same volume of saline solution. After the ten-minute incubation period, additional saline (preheated to 37°C) was added to the incubated solution, and the resulting suspension was measured by the Nanosight NS300. The Nanosight NS300’s laser, temperature and recording settings were identical to those described in Section 2.2.

3.2 Measured Size of Nanoparticles in Blood Plasma

The measured hydrodynamic diameter of nanoparticles after incubation in the various dilutions for each batch of plasma and pure saline can be summarized in Tables C.1 through C.5. The information is visually summarized below in Figure 3.1.

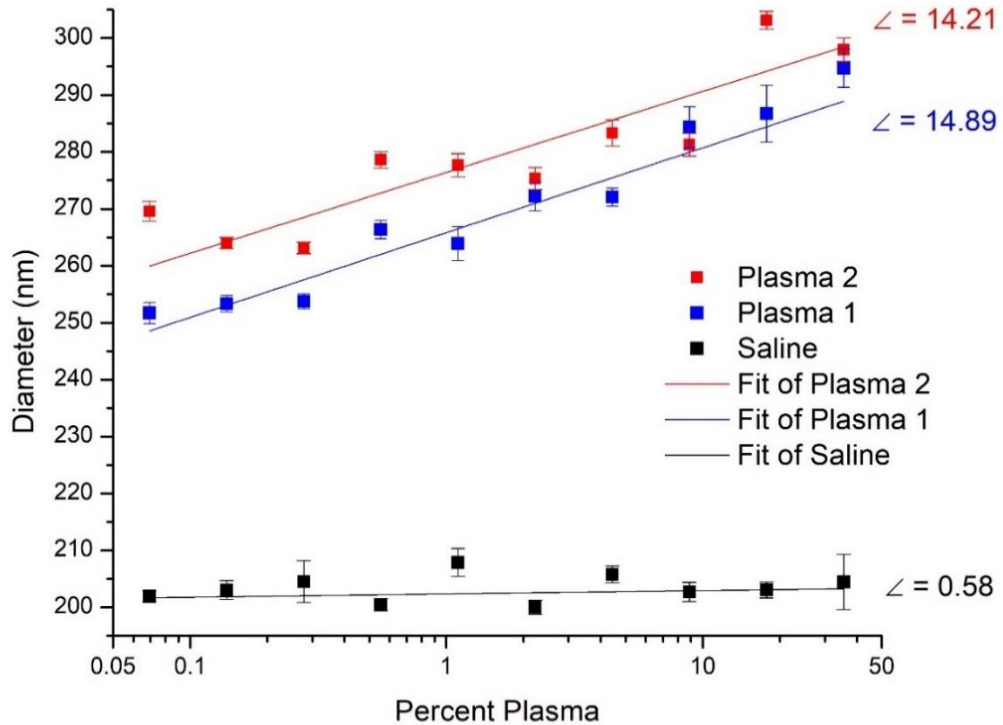


Figure 3.1 Plotted Hydrodynamic Diameter of Polystyrene Nanoparticles After Incubation in Various Dilutions of Blood Plasma and Saline Solution

In addition to graphing the measured hydrodynamic diameter of the nanoparticles, fitted equations were created through linear regression. While these fitted lines appear as linear equations, they are logarithmic equations. For the exact fitted equations and associated R^2 values, see Table C.6. Like Figure 2.6, each data point represents the average size data calculated from three runs of in between seven and 10 measurements taken with each dilution.

Firstly, it is clear that similar trends exist between each batch of plasma. As the solutions become less dilute, the measured size of the nanoparticles in solution increases. Next, some overlap can be seen between data points in the two separate batches. This suggests that different batches of plasma can produce the same sized nanoparticle protein corona for the same dilution, however statistical analysis would be warranted in order to be able to conclude this. Statistical analysis should also be done on each dilution in each batch of plasma in order to conclude the statistical difference between measured nanoparticle hydrodynamic diameters developed in each respective dilution. Finally, both the developed slope and the overall similarities in the measured sizes of nanoparticles in pure saline solutions lead to the assumption that, in pure saline, the particles' hydrodynamic diameters are statistically similar across each dilution. Once again, this warrants statistical analysis to confirm, which will be further discussed in Chapter 4.

CHAPTER 4

STATISTICAL ANALYSIS OF POLYSTYRENE NANOPARTICLE SIZE DATA

4.1 Analysis of Variance

Statistical significance can be determined between two or more groups of raw data through a single factor analysis of variance (ANOVA). This method assesses the amount of variance both within and between group means, and then compares the two values together. From these variances, several parameters are created for analysis. The sum of squares between groups (SSB) represents the variation of group means from the total mean, while the mean of squares between groups (MSB) is the SSB divided by the degrees of freedom between groups. Vice versa, the sum of squares within groups (SSW) represents the sum of squared deviations of the group means and individual observations. Like the MSB, the mean of squares within groups (MSW) is equal to the SSW divided by the degrees of freedom [11].

Next, the ratio of the MSB and MSW is determined, which compares between group variance and within group variance, generally referred to as F. There is also a pre-calculated expected value of F, which is called the critical F value. If the F value is greater than the critical F value, then there are differences between group means that cannot be accounted for by error or chance. Conversely, if the F value is smaller than the critical F value then the two sets of data are considered statistically similar, meaning that any differences in the datasets can be explained by error [11]. Single Factor ANOVA was performed on the two batches of data in Microsoft Excel. First, ANOVA tests were performed on each dilution for pure saline and both batches of plasma to determine

statistical significance between dilutions. Next, an ANOVA test was performed on each batch of plasma to determine the statistical significance between batches.

4.2 ANOVA Test on Dilutions of Pure Saline

The single factor ANOVA test on hydrodynamic diameters of polystyrene particles measured in pure saline is summarized in Table 4.1.

Table 4.1 Single Factor ANOVA Summary of Hydrodynamic Diameters of Nanoparticles Incubated in 10 Incremental Dilutions of Saline

SUMMARY

<i>Groups</i>	<i>Count</i>	<i>Sum</i>	<i>Average</i>	<i>Variance</i>
Dilution 0	25	5111.20	204.45	532.06
Dilution 1	30	6091.10	203.04	57.57
Dilution 2	25	5067.40	202.70	72.64
Dilution 3	30	6173.80	205.79	64.39
Dilution 4	30	6000.40	200.01	46.53
Dilution 5	25	5196.40	207.86	152.26
Dilution 6	30	6014.60	200.49	33.99
Dilution 7	27	5521.70	204.51	359.30
Dilution 8	28	5684.30	203.01	76.77
Dilution 9	30	6057.50	201.92	28.39

ANOVA

<i>Source of Variation</i>	<i>SS</i>	<i>df</i>	<i>MS</i>	<i>F</i>	<i>P-value</i>	<i>F crit</i>
Between Groups	1365.48	9	151.72	1.18	0.31	1.92
Within Groups	34217.49	267	128.16			
Total	35582.97	276				

The calculated F value was 1.18, while the critical F value was 1.92. As the calculated F value is less than the critical F value, the measured hydrodynamic diameters of nanoparticles measured in pure saline are found to be statistically similar to each other. This not only proves that the size of the nanoparticle can indeed be confirmed constant

across each dilution in saline, but it also proves that a significant nanoparticle protein corona is being measured in plasma.

The statistical similarity of the measured hydrodynamic diameters proves that the variation in procedure between each dilution does not cause a size increase in nanoparticles. The only difference between the saline and plasma measurements is the fact that plasma is being added to the incubation solution. Because the dilution procedure does not cause fluctuation in size, the interactions between plasma and the nanoparticles are causing an increase in size. In other words, the Nanosight NS300 is measuring nanoparticles with a sizeable protein corona on them when incubated in plasma.

4.3 ANOVA Test Across Dilutions of Plasma Batches

The single factor ANOVA test on hydrodynamic diameters of polystyrene particles measured in Plasma Batch 1 is summarized in Table 4.2.

Table 4.2 Single Factor ANOVA Summary of Hydrodynamic Diameters of Nanoparticles Incubated in 7 Incremental Dilutions of Plasma 1

SUMMARY

<i>Groups</i>	<i>Count</i>	<i>Sum</i>	<i>Average</i>	<i>Variance</i>
Dilution 0	42.00	12378.67	294.73	474.17
Dilution 1	42.00	12043.03	286.74	1044.95
Dilution 2	35.00	9951.79	284.34	458.34
Dilution 3	28.00	7617.24	272.04	68.54
Dilution 4	25.00	6805.67	272.23	162.85
Dilution 5	28.00	7389.74	263.92	253.56
Dilution 6	49.00	13051.36	266.35	127.60

ANOVA

<i>Source of Variation</i>	<i>SS</i>	<i>df</i>	<i>MS</i>	<i>F</i>	<i>P-value</i>	<i>F crit</i>
Between Groups	30391.05	6.00	5065.18	12.69	0.00	2.14
Within Groups	96597.24	242.00	399.16			
Total	126988.29	248.00				

Unfortunately, raw data was only available for dilutions 0-6 for Plasma 1, the data for which is shown in Table 4.6. Here, the F-value of 12.69 is much larger than the critical F value of 2.14, showing that the measured hydrodynamic diameters of polystyrene nanoparticles incubated in Plasma 1 are statistically different across each dilution. In other words, there is a different sized protein corona developed onto the incubated nanoparticles for each dilution of Plasma 1.

The single factor ANOVA test on hydrodynamic diameters of polystyrene particles measured in Plasma Batch 2 is summarized in Table 4.3.

Table 4.3 Single Factor ANOVA Summary of Hydrodynamic Diameters of Nanoparticles Incubated in 10 Incremental Dilutions of Plasma 2

SUMMARY

<i>Groups</i>	<i>Count</i>	<i>Sum</i>	<i>Average</i>	<i>Variance</i>
Dilution 0	22.00	6555.64	297.98	92.71
Dilution 1	24.00	7274.69	303.11	59.33
Dilution 2	23.00	6468.84	281.25	92.27
Dilution 3	26.00	7348.24	282.62	134.59
Dilution 4	20.00	5506.39	275.32	73.45
Dilution 5	30.00	8329.20	277.64	123.64
Dilution 6	25.00	6962.01	278.48	59.05
Dilution 7	21.00	5525.44	263.12	21.51
Dilution 8	23.00	6072.14	264.01	23.39
Dilution 9	26.00	7008.81	269.57	74.40

ANOVA

<i>Source of Variation</i>	<i>SS</i>	<i>df</i>	<i>MS</i>	<i>F</i>	<i>P-value</i>	<i>F crit</i>
Between Groups	35419.40	9.00	3935.49	50.54	0.00	1.92
Within Groups	17908.96	230.00	77.87			
Total	53328.36	239.00				

Once again, the F-value of 50.54 is much larger than the critical F value of 1.92, showing that the measured hydrodynamic diameters of polystyrene nanoparticles incubated in Plasma 2 are also statistically different across each dilution. Because of the statistical difference displayed across dilutions 0-10 in Tables 4.2 and 4.3, the trends shown in Figure 3.1 can be confirmed. As each nanoparticle suspension becomes less dilute with respect to plasma, the measured hydrodynamic diameter of nanoparticles increases.

4.4 ANOVA Test Across Separate Plasma Batches

The single factor ANOVA test on the average hydrodynamic diameters of polystyrene particles in each dilution measured in Plasma Batch 1 and Plasma Batch 2 is summarized in Table 4.4.

Table 4.4 Single Factor ANOVA Summary of Measured Hydrodynamic Diameters of Nanoparticles Incubated in Plasma 1 and Plasma 2

SUMMARY				
<i>Groups</i>	<i>Count</i>	<i>Sum</i>	<i>Average</i>	<i>Variance</i>
Plasma 2	10	2699.16	269.92	225.82
Plasma 1	10	2793.93	279.39	171.74

ANOVA						
<i>Source of Variation</i>	<i>SS</i>	<i>df</i>	<i>MS</i>	<i>F</i>	<i>P-value</i>	<i>F crit</i>
Between Groups	449.06	1	449.06	2.26	0.15	4.41
Within Groups	3578.01	18	198.78			
Total	4027.07	19				

The F-value of 2.26 is obviously smaller than the critical F-value of 4.41, meaning that the measured hydrodynamic diameters of nanoparticles in their respective dilutions are statistically similar across each batch of plasma. This confirms the visual similarities between each set of data in plasma shown in Figure 3.1, and that two batches of plasma from the same species will produce similar sized protein coronas. The statistical analysis of the hydrodynamic diameters of nanoparticles in each dilution was useful, however it would be more useful to be able to characterize data specifically describing the size of the protein corona.

CHAPTER 5

AVERAGE PROTEIN CORONA THICKNESS ANALYSIS

5.1 Average Thickness of Developed Protein Coronas

According to the definition of the protein corona discussed in Chapter 1, the protein corona can be thought of as a shell around the nanoparticle in solution. Because the Nanosight NS300 assumes that all measured particles are perfectly spherical, that same assumption can be applied to a particle's protein corona. It is important to note that it is not guaranteed that every nanoparticle and its resulting corona will be perfectly spherical in shape. By subtracting the true measured size of the nanoparticles in saline for each dilution from the hydrodynamic diameter of the particle and protein corona and then dividing the resultant number in half, the actual thickness of the protein corona was able to be determined. This information is summarized in Tables C.7 and C.8 for both batches of blood plasma used.

The thickness ranges in between 20 and 50 nanometers, with standard error that is once again very low, ranging from 1 to 5 nm. While these thicknesses seem negligible in terms of size, they become very significant when taking the size of the nanoparticles being used into account. In terms of percent change, incubation of nanoparticles in blood plasma was found to increase the overall nanoparticle diameter from anywhere between 20% and 50% of its original size. This change is substantial and based upon the trends seen in Figure 3.1, when a nanoparticle is incubated in undiluted blood plasma in a human body, this change could increase even more. The information in Tables C.7 and C.8 is visually

summarized in Figure 5.1

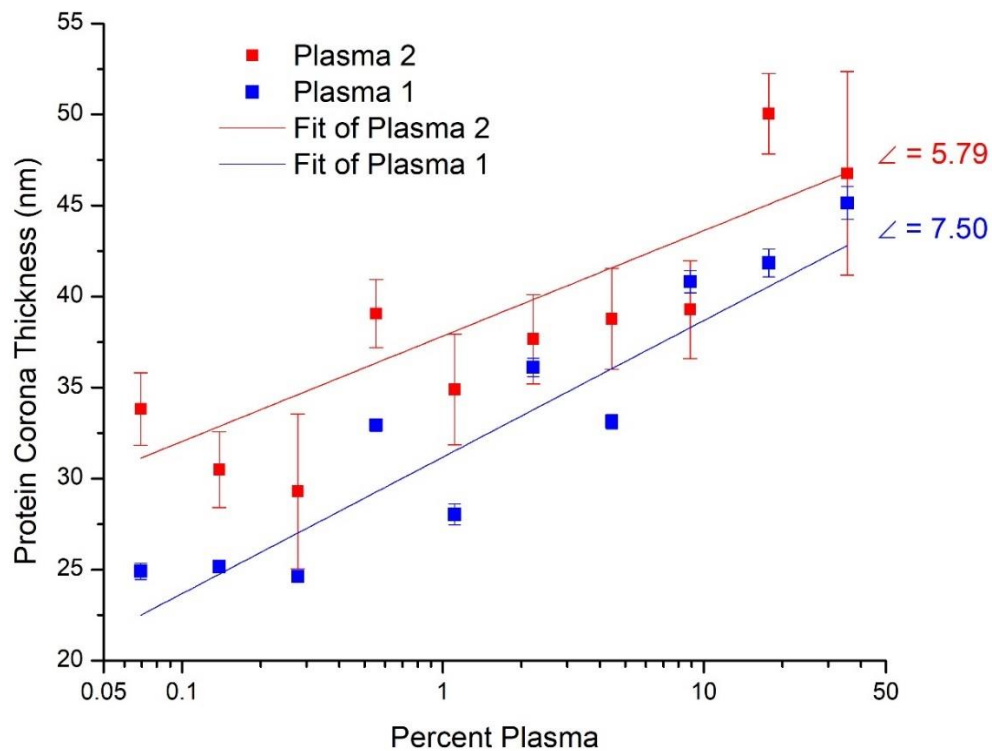


Figure 5.1 Average Thickness of Protein Coronas After Incubation in Various Dilutions of Blood Plasma and Saline Solution for Plasma 1 and Plasma 2

Like Figure 3.1, there is a clearly positive trend portrayed by the data. As the plasma solutions become less dilute, the resultant protein corona becomes thicker. This makes sense, as the protein corona thickness is directly related to the overall hydrodynamic diameter of the nanoparticles in incubation. This figure just provides a more streamlined way of looking at the data. More detailed information about the logarithmic relationships derived by linear regression can be found in Table 5.1.

Table 5.1 Fitted Equations Developed from the Linear Regression of the Data Plotted in Figure 5.1

Data Set	Equation	R ²
Plasma 2	$Y = 6.14 \times \log_{10}(X) + 36.81$	0.73
Plasma 1	$Y = 7.82 \times \log_{10}(X) + 31.74$	0.88

Once again, overlap can be seen between thickness data points in the two separate batches of plasma. This suggests that different batches of plasma can produce protein corona with similar thickness. Based upon the statistical analysis done on the hydrodynamic diameters of the incubated nanoparticles between batches of plasma, it is assumed that this conclusion is accurate, however more statistical analysis would be warranted. Statistical analysis should also be done on each dilution in each batch of plasma in order to conclude the difference between protein corona thickness developed in each respective dilution of each batch of plasma. Finally, statistical analysis should be completed on the linear regression equations in Table 5.1 to determine their statistical significance.

5.2 ANOVA Tests on Average Protein Corona Thickness

The ANOVA test on the average protein corona thickness of nanoparticles incubated in each respective dilution of Plasma 1 is summarized in Table 5.2.

Table 5.2 Single Factor ANOVA Summary of Average Protein Corona Thickness of Nanoparticles Incubated in 7 Incremental Dilutions of Plasma 1

Summary				
<i>Groups</i>	<i>Count</i>	<i>Sum</i>	<i>Average</i>	<i>Variance</i>
Dilution 0	42.00	1895.89	45.14	118.54
Dilution 1	42.00	1757.67	41.85	261.24
Dilution 2	35.00	1428.82	40.82	114.58
Dilution 3	28.00	927.56	33.13	17.14
Dilution 4	25.00	902.71	36.11	40.71
Dilution 5	28.00	784.83	28.03	63.39
Dilution 6	29.00	1613.68	32.93	31.9

ANOVA						
<i>Source of Variation</i>	<i>SS</i>	<i>df</i>	<i>MS</i>	<i>F</i>	<i>P-Value</i>	<i>F crit</i>
Between Groups	7747.38	6.00	1291.23	12.94	0.00	2.14
Within Groups	24149.31	242.00	99.79			
Total	31896.69	248.00				

Once again, raw data was only available for dilutions 0-6 for Plasma 1, the data for which is shown in Table C.3. Here, the F-value of 12.94 is much larger than the critical F value of 2.14, showing that average protein corona thickness of polystyrene nanoparticles incubated in Plasma 1 are statistically different across each dilution. In other words, there is a different sized protein corona developed onto the incubated nanoparticles for each dilution of Plasma 1. Because the average protein corona thickness is directly related to the measured hydrodynamic size of nanoparticles in suspension, this result was expected.

The ANOVA test on the average protein corona thickness of nanoparticles incubated in each respective dilution of Plasma 2 is summarized in Table 5.3.

Table 5.3 Single Factor ANOVA Summary of Average Protein Corona Thickness of Nanoparticles Incubated in 10 Incremental Dilutions of Plasma 2

SUMMARY

<i>Groups</i>	<i>Count</i>	<i>Sum</i>	<i>Average</i>	<i>Variance</i>
Dilution 0	22.00	1028.89	46.77	23.18
Dilution 1	24.00	1200.90	50.04	14.83
Dilution 2	23.00	903.42	39.28	23.07
Dilution 3	27.00	1046.72	38.77	35.69
Dilution 4	20.00	753.06	37.65	18.36
Dilution 5	30.00	1046.76	34.89	30.91
Dilution 6	26.00	1015.48	39.06	14.27
Dilution 7	21.00	615.39	29.30	5.38
Dilution 8	23.00	701.45	30.50	5.85
Dilution 9	26.00	879.49	33.83	18.60

ANOVA

<i>Source of Variation</i>	<i>SS</i>	<i>df</i>	<i>MS</i>	<i>F</i>	<i>P-value</i>	<i>F crit</i>
Between Groups	8878.91	9.00	986.55	50.12	0.00	1.92
Within Groups	4566.37	232.00	19.68			
Total	13445.28	241.00				

The F-value of 50.12 is much larger than the critical F value of 1.92, showing that the average protein corona thickness of polystyrene nanoparticles incubated in Plasma 2 are also statistically different across each dilution. Because of the statistical difference displayed across dilutions in Tables 5.2 and 5.3, the trends shown in Figure 5.1 can be confirmed. As each nanoparticle suspension becomes less dilute with respect to plasma, the average thickness of the protein corona developed onto nanoparticles increases.

The ANOVA test on average protein corona thickness of nanoparticles incubated in dilutions across each batch of plasma used is summarized in Table 5.4

Table 5.4 Single Factor ANOVA Summary of Average Protein Corona Thickness of Nanoparticles Incubated in Plasma 1 and Plasma 2

SUMMARY

<i>Groups</i>	<i>Count</i>	<i>Sum</i>	<i>Average</i>	<i>Variance</i>
Plasma 2	10	380.08	38.01	42.69
Plasma 1	10	332.70	33.27	57.52

ANOVA

<i>Source of Variation</i>	<i>SS</i>	<i>df</i>	<i>MS</i>	<i>F</i>	<i>P-value</i>	<i>F crit</i>
Between Groups	112.27	1	112.27	2.24	0.15	4.41
Within Groups	901.93	18	50.11			
Total	1014.19	19				

The F-value of 2.24 is obviously smaller than the critical F-value of 4.4, meaning that the average protein corona thickness of nanoparticles incubated in their respective dilutions are statistically similar across each batch of plasma. This confirms the visual similarities between each set of data in plasma shown in Figure 3.1, and that two batches of plasma from the same species will produce similar sized overall protein coronas. Being able to compare overall protein coronas is useful, however, as discussed in Chapter 1, protein corona is characterized by both the hard and soft corona. Therefore, it is important to be able to differentiate between these two components in these measurements.

5.3 Statistical Analysis of Average Protein Corona Thickness Regression

Table 5.1 displays the equations of the fitted lines plotted on Figure 5.1, comparing the average protein corona thickness to the logarithm of the percentage of plasma present in each dilution. The two equations look visually similar on Figure 5.1 and appear to have comparable slopes and intercepts. Based upon the definition of a protein corona, it was

determined that these linear equations could be used to characterize the size of the hard and soft protein coronas within each batch of plasma.

It was determined that the slope of the linear equation determines the effect of the soft corona on the overall average protein corona thickness, while the constant of the linear equation determines the effect of the hard corona on the overall average protein corona thickness. Recalling the definition of protein corona, the hard corona is comprised of one layer of proteins that are directly bound to the surface of the nanoparticle. Therefore, it can be assumed that compared to the thickness of the overall protein corona, which is around 50 nanometers, the small thickness of the hard corona will stay fairly constant across the protein coronas developed in each dilution. In an equation that determines the overall thickness, it should be represented by the unchanging constant. The slope of the equation determines the change in the overall thickness of the protein corona, and as the solutions become less dilute the thickness increases. Therefore, it can be assumed that the nanoparticles incubated in the less dilute solutions have the same sized hard corona but have larger soft coronas. Therefore, as the slope accounts for variation between dilutions, it therefore represents the size of the soft corona.

In order to analyze the difference between the hard and soft corona across batches of plasma, statistical analysis needed to be performed on the two linear regression equations. Statistical analysis of slopes and constants produced through linear regression can be completed through hypothesis testing. For both the slopes and the constants, the two data sets were separated by a categorical variable, which identified which set of plasma the data was being used for incubation.

For the developed slopes, a fitted regression was developed for each set of data while taking an interaction effect into account. Interaction effects display the effects of factors on each dependent measure, or the size/thickness of the particle/protein corona, showing that the impact of a factor depends on the level of another factor [12]. In this case, the interaction effect is the product of the log of the percentage of plasma in solution and the categorical variable, “Plasma Batch”, with “A” representing Plasma 2 and “B” representing Plasma 1. This procedure provides two linear fits with which the developed coefficients (or slopes) could be assessed. Figure 5.2 shows an example of the results of a hypothesis test on two sets of developed slopes and constants [18].

Regression Equation		Coefficients					
Condition		Term	Coef	SE Coef	T-Value	P-Value	VIF
A	Output = 9.099 + 1.5359 Input	Constant	9.099	0.980	9.29	0.000	
		Input	1.5359	0.0823	18.67	0.000	2.00
		Condition					
		B	-2.36	1.39	-1.70	0.093	4.48
B	Output = 6.740 + 2.0050 Input	Input*Condition					
		B	0.469	0.116	4.03	0.000	5.48

Figure 5.2 Minitab Results from a Coefficient Comparison Between Two Independently Developed Coefficients Using a Hypothesis Test.

Source: Ogee, Agnes, et al. “How to Compare Regression Slopes.” *The Minitab Blog*, Minitab, 13 Jan. 2016, blog.minitab.com/blog/adventures-in-statistics-2/how-to-compare-regression-lines-between-different-models.

A couple of things should be seen in a coefficient table such as above. When considering the significance of the slopes, the cell of value is the intersection between “Input*Condition”, which is the interaction effect, and P-Value. The hypothesis test starts with the hypothesis that the two developed slopes of the linear regressions are equal, which would be supported by a P-value of greater than the confidence interval at which this analysis was ran, which for all intents and purposes will be 0.05 [12]. In Figure 5.2, the P-

Value of the interaction term is 0, which is less than 0.05, and therefore the null hypothesis can be rejected, and the two slopes can be considered statistically significant [18].

When considering the significance of the constants, the cell of value is the intersection between “Condition” and P-Value. The hypothesis test starts with the hypothesis that the two developed constants of the linear regressions are equal, which would be supported by a P-value greater than the confidence interval at which this analysis was ran, which for all intents and purposes will be 0.05. In Figure 5.2, the P-Value of the interaction term is 0, which is less than 0.05, and therefore the null hypothesis can be rejected, and the two coefficients can be considered statistically significant. These principles will now be provided to the previously discussed data [18]. Table 5.5 displays the statistical analysis of the linearly regressed equations fit to the average protein corona thickness of nanoparticles incubated in Plasma 1 and Plasma 2.

Table 5.5 Regression Analysis of Fitted Equations Developed from the Data Plotted in

Term	Coefficient	Standard Error of Coefficient	T-Value	P-Value	VIF
Constant	36.810	1.030	35.63	0.000	-
Logarithm of Plasma Percentage	6.140	1.170	5.27	0.000	2.000
Plasma Batch: B	-5.070	1.460	-3.470	0.003	1.050
Logarithm of Plasma Percentage* Plasma Batch: B	1.680	1.650	1.020	0.332	2.050

Obviously, the P-Value associated with the interaction effect (Plasma Concentration*Plasma Batch B) is larger than the confidence interval of 0.05, with a value of 0.332. This means that the null hypothesis cannot be rejected, and that there is no

statistical significance between the two slopes produced by the linear regression of the average protein corona thickness plotted against the logarithm of the percentage of plasma present in each dilution. Because there is no statistical significance between the two slopes produced by linear regression of the average protein corona thickness for each plasma batch, it can be concluded that the soft corona has the same effect on the overall protein corona for different batches of plasma from the same species. In other words, each batch of plasma should have similarly sized soft protein coronas.

The P-Value associated with the Plasma Batch value is smaller than the confidence interval of 0.05, with a value of 0.003. This means that the null hypothesis can be rejected, and that there is a statistical significance between the two constants produced by the linear regression of the average protein corona thickness plotted against the logarithm of the percentage of plasma present in each dilution. Because there is a statistical significance between the two constants produced by linear regression of the average protein corona thickness for each plasma batch, it can be concluded that the hard corona has a different effect on the overall protein corona for different batches of plasma from the same species. In other words, each batch of plasma should have different sized hard protein coronas.

CHAPTER 6

FUTURE WORK

6.1 Dilution Experiment Expansion

The dilution experiment was an excellent springboard towards understanding protein corona composition, however much more work needs to be done to confirm some of the discovered trends. In order to determine the validity of future use of the Nanosight NS300, experiments will need to be done in which nanoparticles are incubated in undiluted blood plasma. This will allow for a more accurate simulation of the interactions between blood plasma proteins and nanoparticle drug delivery solutions. As the goal of these experiments is to simulate flow of nanoparticle drug systems within the human body, the ability to measure the hydrodynamic diameter of nanoparticles in undiluted plasma is crucial to future implementation.

Different types of blood plasma must be tested in order to confirm the existence of the claimed trends across different species. Because human blood plasma is a biohazard and requires special engineering controls to safely use, it would be wise to test the claim on another animal. Figure 6.1 shows a comparison of the results of zone electrophoresis between ox (bovine) plasma and human plasma.

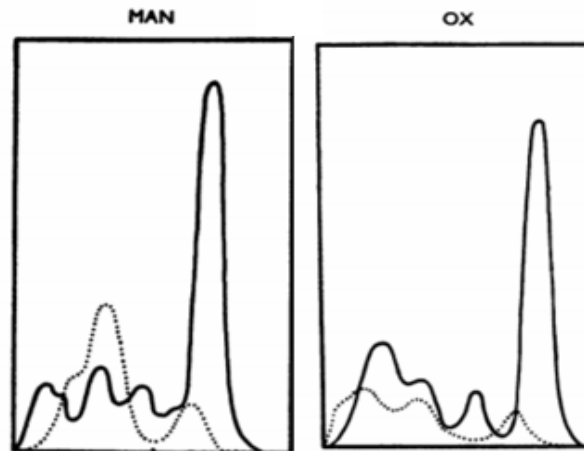


Figure 6.1 Comparison Between Human and Ox Blood Plasma Using Zone Electrophoresis.

Source: Source: Morris, Bede, and F. C. Courtice. "The Protein And Lipid Composition Of The Plasma Of Different Animal Species Determined By Zone Electrophoresis And Chemical Analysis." *Quarterly Journal of Experimental Physiology and Cognate Medical Sciences*, vol. 40, no. 2, 7 Nov. 1955, pp. 127–137., doi:10.1113/expphysiol.1955.sp001104.

Like goat blood plasma, bovine plasma is quite similar to human blood plasma. Both plasma types contain significant amounts of fibrinogen, gamma, beta and alpha globulins and albumin. Zone electrophoresis also migrated the lipids contained in bovine plasma into two distinct areas, despite human lipids being migrated into three. However, both lipid migrations contained a zone localized around the albumin and beta-globulin protein areas [16]. Bovine plasma is safer to use than human blood, and its use will be a greater step forward in either confirming or denying some of the trends seen in goat plasma across different types of plasma. While the goal still remains to be able to control protein corona in human plasma, use of all other plasma types still acts as an intermediary to performing experiments using human plasma.

Different nanoparticles with different surface chemistries must be used in future experiments. The importance of surface charge and various physical characteristics of nanoparticle systems in protein corona formation was discussed in Chapter 1, and it remains an important task to understand the roles of these traits in protein corona development. A commonly used polymer in nanoparticle drug delivery systems is poly(lactic-co-glycolic acid), also known as PLGA. Another popular substance used is gold nanoparticles, which are often used in cancer remediation because of the inherent stability to assembly and malleable surface properties [9]. Another option is changing the surface chemistry of the PLGA nanoparticles by using polyethylene glycol, or PEG, which theoretically masks nanoparticles from proteins in blood plasma [1]. Not only will varying the surface chemistry and types of nanoparticle systems provide more information upon nanoparticle and plasma protein interactions, but it could lead towards information on the most efficient and useful nanoparticle system. PEGylated particles have already been synthesized using 1K, 5K, 10K and 30K PEG, and future experiments will be done on those particles in order to determine their influence on the development of the protein corona.

6.2 Determining Protein Corona Composition

To prove the theories discussed from the results of the hypothesis testing, one would have to be able to physically distinguish between the hard and soft corona. In *Microfluidic Examination of the 'Hard' Biomolecular Corona Formed on Engineered Particles in Different Biological Milieu*, Weiss discusses a technique for washing nanoparticles after incubation. This washing, theoretically, would remove the soft corona from the

nanoparticles, as it is weakly bound to the particle. However, the proteins that make up the hard corona should be able to retain their bonds to the particle. By this logic, one would be able to measure the size of only the particle and the hard corona. The sizes of these washed particles could then be compared from dilution to dilution, and if the theory holds up, would prove that the size of each nanoparticle and hard corona would be constant regardless of the amount of blood plasma each nanoparticle is incubated in [23]. Therefore, any hydrodynamic diameter variation seen in Figure 3.1 or thickness variation seen in Figure 5.1 would be a direct result in a change in the size of the soft protein corona.

Weiss also discusses the possible determination of the composition of the hard corona after the washing step through gel electrophoresis and mass spectrometry. Gel electrophoresis would allow the proteins present on the hard corona to be separated by atomic mass. Mass spectrometry would be able to determine the relative amounts of each protein in the hard protein corona [23]. These experiments are extremely important for multiple reasons.

First, understanding the proteins that make up the protein corona could allow different measures to be taken to avoid the binding of those proteins, such as changing nanoparticle surface chemistry. Knowing the relative amounts of the proteins present in the protein corona will give more information on how the protein corona is formed, and a better inherent understanding of the clashing between Vroman's Effect and Brownian Motion. Finally, knowing the composition of individual protein coronas would give information on the binding affinities of individual proteins, which would help future design of drug delivery nanoparticles and even assist in perfecting the quantification of the effective binding coefficient of plasma. This information could be vital to the implementation of

nanoparticle systems as drug delivery solutions, and therefore experiments to determine protein corona composition are vital for future research.

6.3 Binding Affinity

A successive project resulting from this work would be to calculate the binding affinity of blood plasma to nanoparticles. According to experiments done by Zhang et al., the binding affinity is calculated using calorimetry data from nanoparticle incubation in blood plasma, attained using Isothermal Titration Calorimetry. Binding affinities in the literature are calculated for individual protein solutions and nanoparticles incubated within them, however the goal is to be able to calculate said binding affinities for overall batches of plasma containing many different proteins and then comparing the affinities for similarities [25].

The binding affinity can be calculated from the Gibb's Free Energy, which can be calculated from the enthalpy and entropy measured through calorimetry data. The equation for the binding affinity is $\Delta G = RT \times \ln(k_A)$, Where ΔG is the Gibb's Free Energy, R is the universal gas constant, T is the absolute temperature and k_A is the binding affinity of the solvent. By comparing the binding affinities of batches of plasma with those from individual protein solutions it is believed that the composition of the protein corona will be able to be determined, or at least easier to characterize. A goal is also to measure these binding affinities onto different types of nanoparticles, such as the newly developed PEGylated PLGA particles or even gold nanoparticles [25].

CHAPTER 7

CONCLUSION

While the experiments and resultant analysis discussed above give updated and useful information about protein corona, it is clear that many more experiments will have to be carried out before nanoparticle drug delivery systems are efficient. The results of the dilution experiment generated some interesting claims and trends, all of which will be referred to and implemented in further work. That being said, there is definitely a future for nanoparticle drug delivery in pharmaceutical practice.

Firstly, NTA is a more reliable method of measuring the hydrodynamic diameter of nanoparticles in solutions containing blood plasma. It was made clear that measurements from DLS were unreliable and theoretically inaccurate even at dilutions containing a small amount of goat blood plasma. The measurements using the Nanosight NS300 appeared accurate up to the 35.5% blood plasma solution that has been tested so far, however the machine's fluorescent capabilities should allow for the hydrodynamic diameter of nanoparticles to be measured in undiluted blood plasma, which is crucial, as that is what nanoparticles will be in when implemented in the body.

The dilution experiment proved the existence of protein corona around polystyrene nanoparticles upon incubation in blood plasma. The statistical similarity between the hydrodynamic diameters of polystyrene nanoparticles across all ten "dilutions" of pure saline proved that neither the saline nor the dilution preparation should have any effect on the size of the nanoparticles, and all size changes are a result of the interactions between the nanoparticles and the blood plasma. On the other hand, the statistical significance of

the measured diameters of polystyrene nanoparticles across all ten dilutions of plasma in each batch prove that each dilution produces a different sized protein corona.

After careful statistical analysis using single factor ANOVA, it was determined that the both the measured hydrodynamic diameters of and average protein corona thickness surrounding each polystyrene nanoparticle were considered statistically similar for both batches of goat plasma used. Hypothesis testing on the slopes and constants generated by regression showed that while the slopes were statistically similar, the developed constants were not. This can be translated in terms of the soft and hard corona, saying that the size of the soft corona will stay generally constant and the hard corona will change between batches of blood plasma from the same species, specifically goat plasma. In order to actually prove this claim, more experiments will have to be done in goat plasma, as a sample size of two batches simply is not enough to make any accurate assumptions.

Finally, future work must be done in order to ensure the massive potential of nanoparticle drug delivery is reached. More experiments must be done using blood plasma from different species, different types of nanoparticles, different nanoparticle surface charges, and finally using human blood plasma. The composition of developed protein coronas can be determined from gel electrophoresis and mass spectrometry, and therefore experiments should be designed to determine said composition in order to understand the best way to inhibit nanoparticle interactions with specific proteins within the plasma. Finally, calorimetry data of the development of a protein corona upon incubation of nanoparticles should be collected in order to calculate binding affinities of plasma onto specific nanoparticle surfaces.

APPENDIX A

Dynamic Light Scattering

A.1 Malvern Zetasizer Nano ZS

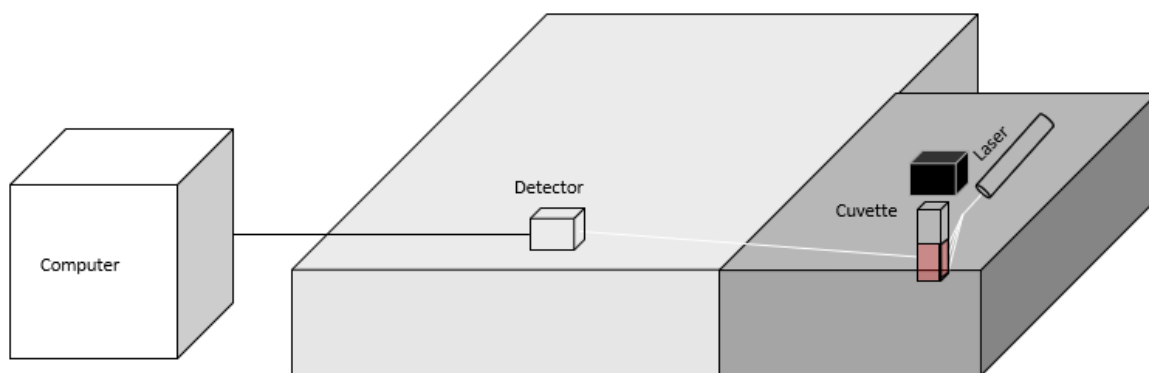


Figure A.1 Schematic of Malvern Zetasizer Nano ZS

The above schematic shows the operation of the Malvern Zetasizer Nano ZS. A cuvette containing a suspension (in this case blood plasma dilutions with polystyrene nanoparticles) is placed into the machine and the lid is closed. A laser then shines light through the samples, which will then be scattered by any particles that come into contact with it. This scattered light is reflected towards a detector, which will send a signal to the computer. The result of this system is the measured hydrodynamic diameter of the nanoparticle as a function of the intensity of scattered light sent to the detector.

A.2 Dilution Experiment

Raw data from DLS is in the form of the correlation function, which the software fits to produce the size distribution as the intensity of scattered light plotted against the measured hydrodynamic diameters of the particles in suspension. The fit to the correlation function developed in order to create the size distribution is described by the “Expert Advice” Tab in the Zetasizer’s user interface. This tab describes the goodness of fit of the size data, and where the sample quality was good enough to produce an accurate function. The DLS results for each of the separate runs are displayed in the following figures.

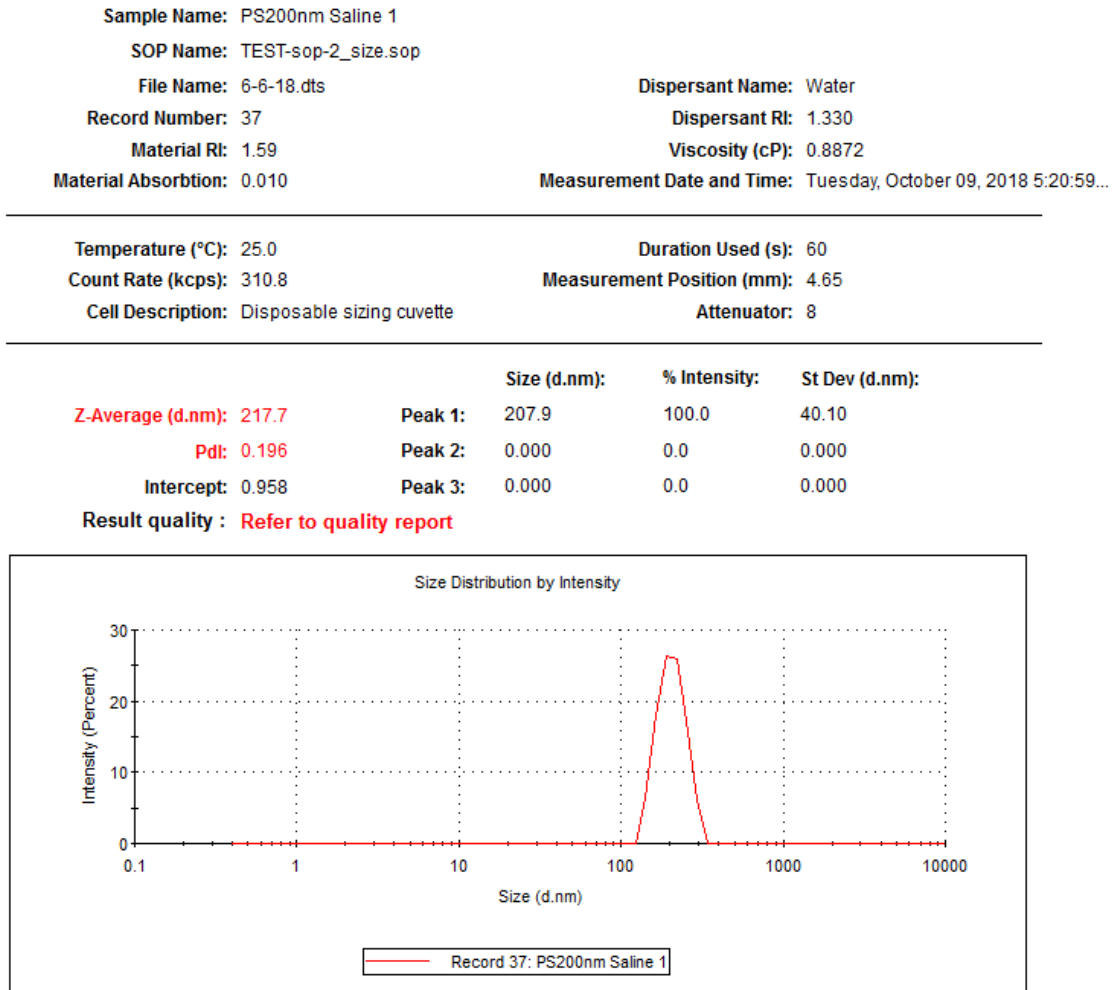


Figure A.2 DLS Results from Polystyrene Nanoparticles Incubated in Saline, Run #1

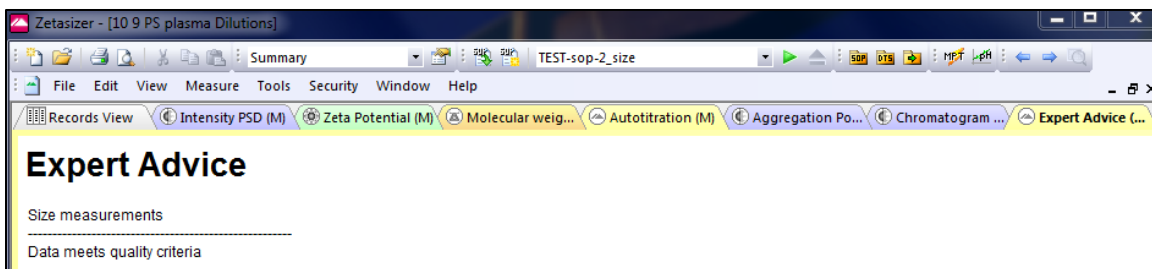


Figure A.3 Description of Data Quality for Saline, Run #1

Sample Name: PS200nm Saline 2	Dispersant Name: Water
SOP Name: TEST-sop-2_size.sop	Dispersant RI: 1.330
File Name: 6-6-18.dts	Viscosity (cP): 0.8872
Record Number: 38	Measurement Date and Time: Tuesday, October 09, 2018 5:23:13...
Material RI: 1.59	
Material Absorbance: 0.010	

Temperature (°C): 25.0	Duration Used (s): 60
Count Rate (kcps): 307.4	Measurement Position (mm): 4.65
Cell Description: Disposable sizing cuvette	Attenuator: 8

	Size (d.nm):	% Intensity:	St Dev (d.nm):
Z-Average (d.nm): 219.1	Peak 1: 233.3	100.0	59.01
PdI: 0.060	Peak 2: 0.000	0.0	0.000
Intercept: 0.947	Peak 3: 0.000	0.0	0.000

Result quality : Good

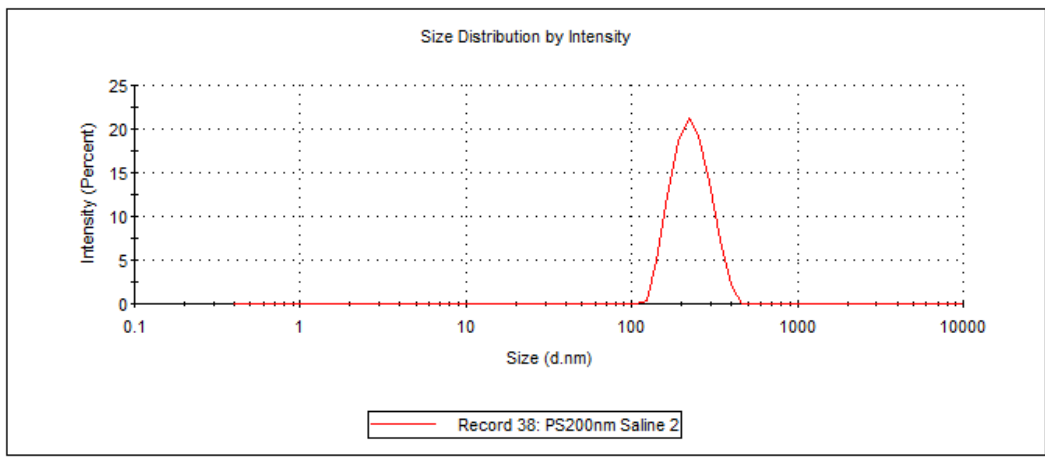


Figure A.4 DLS Results from Polystyrene Nanoparticles Incubated in Saline, Run #2

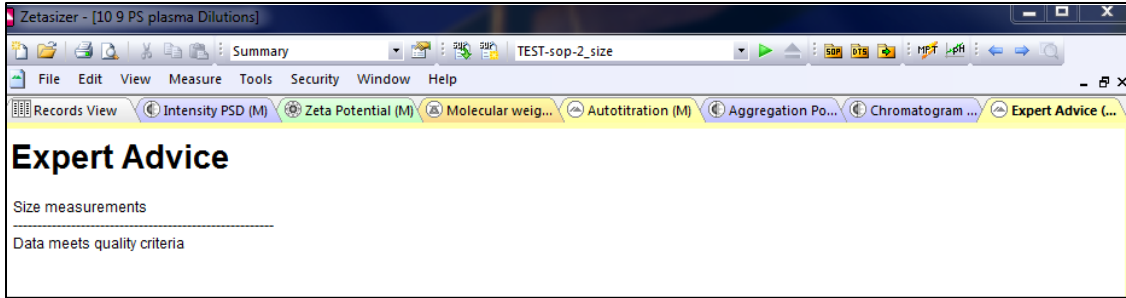


Figure A.5 Description of Data Quality for Saline, Run #2

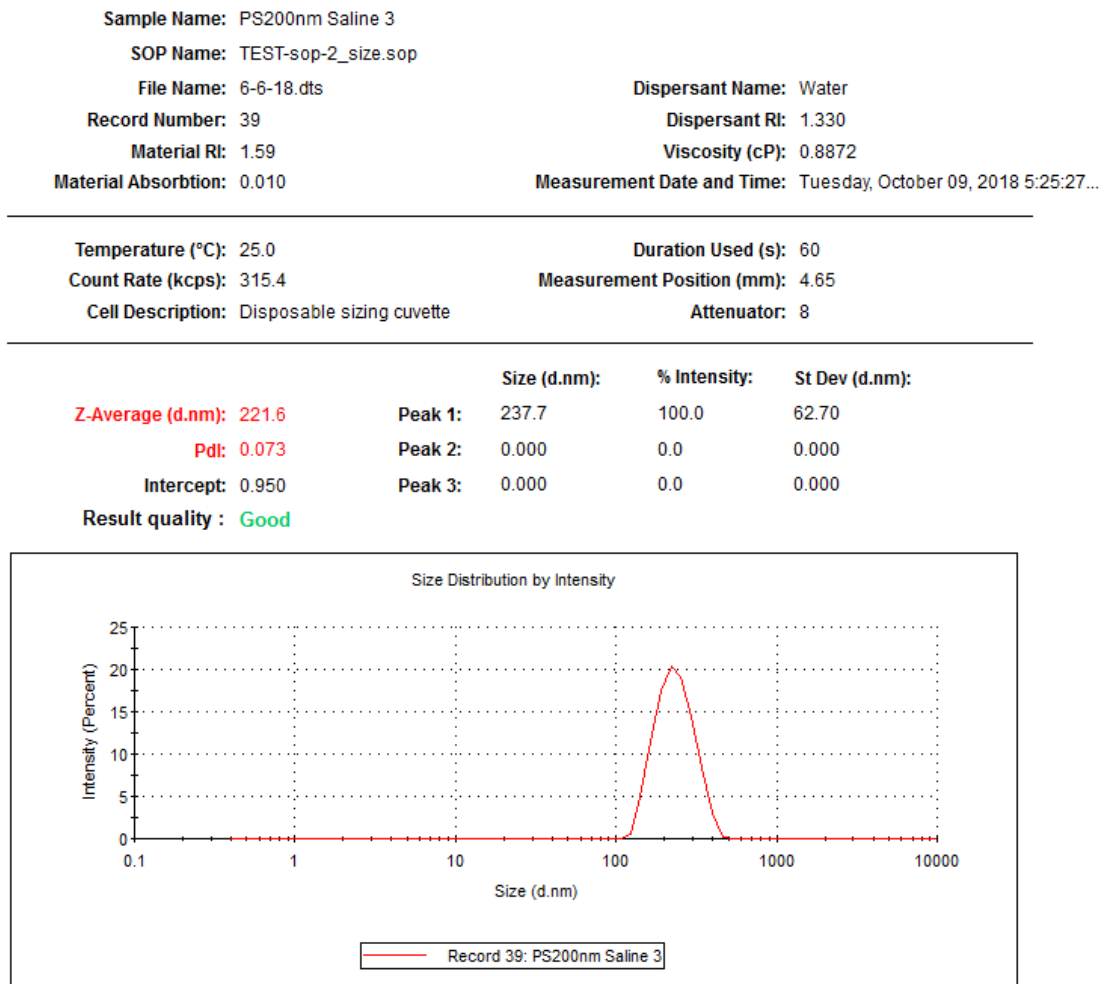


Figure A.6 DLS Results from Polystyrene Nanoparticles Incubated in Saline, Run #3

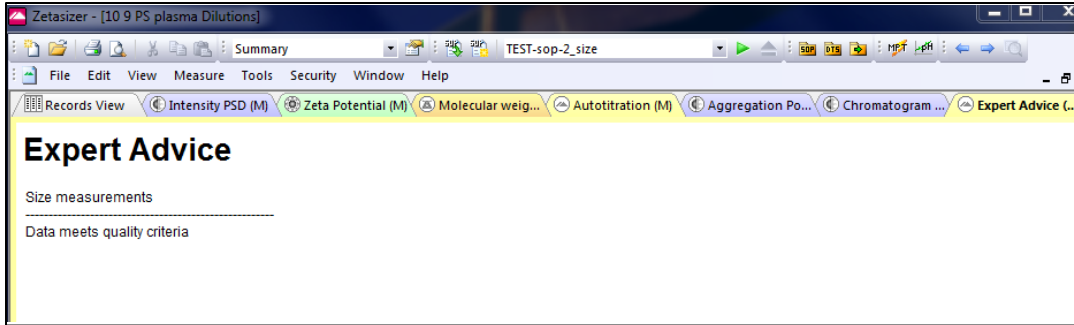


Figure A.7 Description of Data Quality for Saline, Run #3

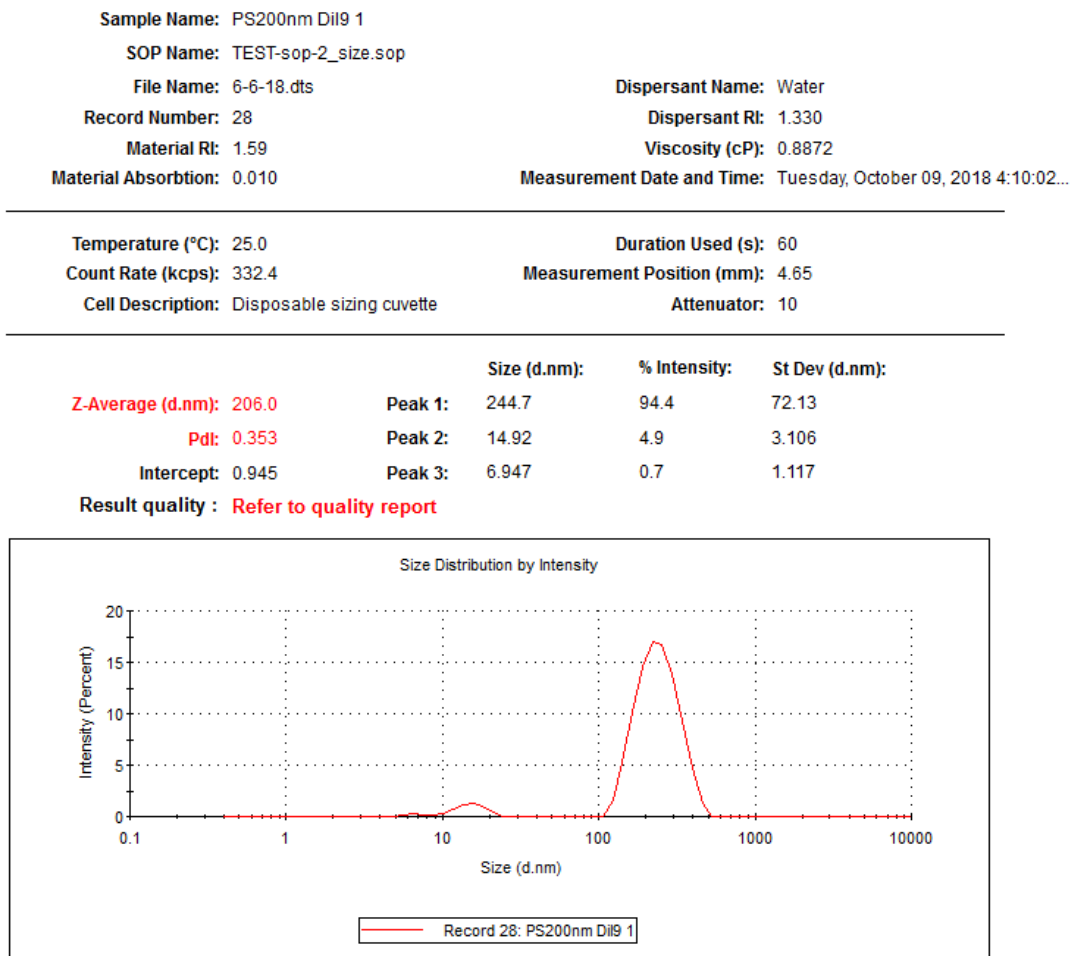


Figure A.8 DLS Results from Polystyrene Nanoparticles Incubated in Dilution 9, Run #1

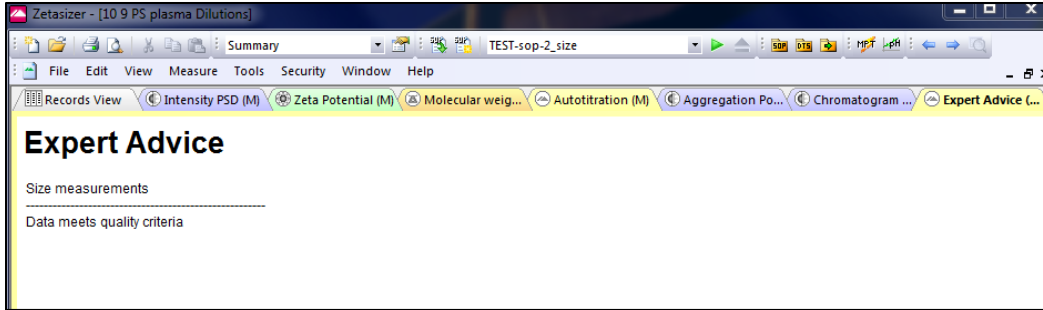


Figure A.9 Description of Data Quality for Dilution 9, Run #1

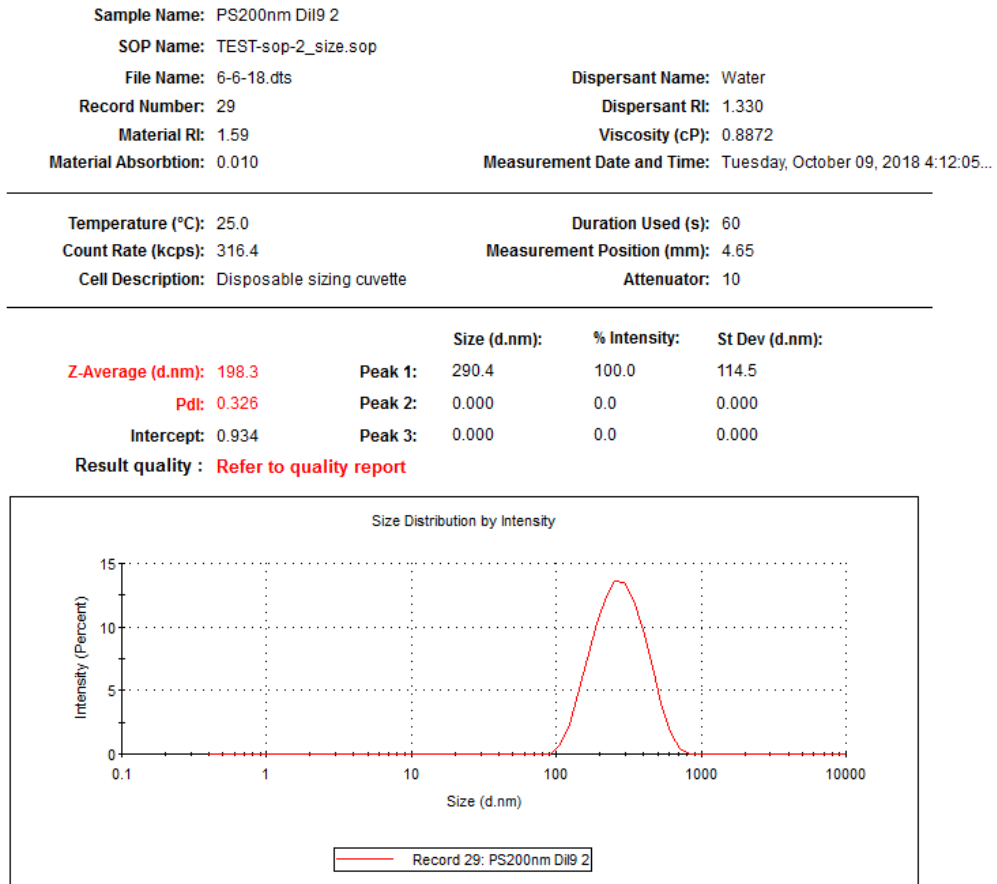


Figure A.10 DLS Results from Polystyrene Nanoparticles Incubated in Dilution 9, Run #2

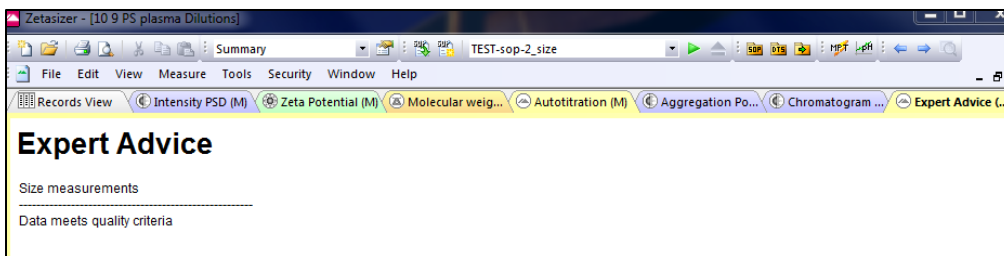


Figure A.11 Description of Data Quality for Dilution 9, Run #2

Sample Name: PS200nm Dil9 3	Dispersant Name: Water
SOP Name: TEST-sop-2_size.sop	Dispersant RI: 1.330
File Name: 6-6-18.dts	Viscosity (cP): 0.8872
Record Number: 30	Measurement Date and Time: Tuesday, October 09, 2018 4:14:09...
Material RI: 1.59	
Material Absorbance: 0.010	
Temperature (°C): 25.0	Duration Used (s): 60
Count Rate (kcps): 323.8	Measurement Position (mm): 4.65
Cell Description: Disposable sizing cuvette	Attenuator: 10

	Size (d.nm):	% Intensity:	St Dev (d.nm):
Z-Average (d.nm): 188.0	Peak 1: 253.2	100.0	84.61
Pdl: 0.296	Peak 2: 0.000	0.0	0.000
Intercept: 0.928	Peak 3: 0.000	0.0	0.000

Result quality : Refer to quality report

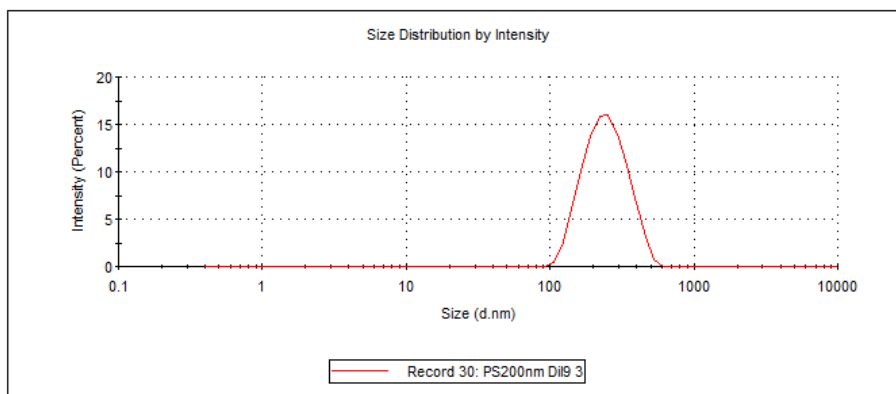


Figure A.12 DLS Results from Polystyrene Nanoparticles Incubated in Dilution 9, Run #3

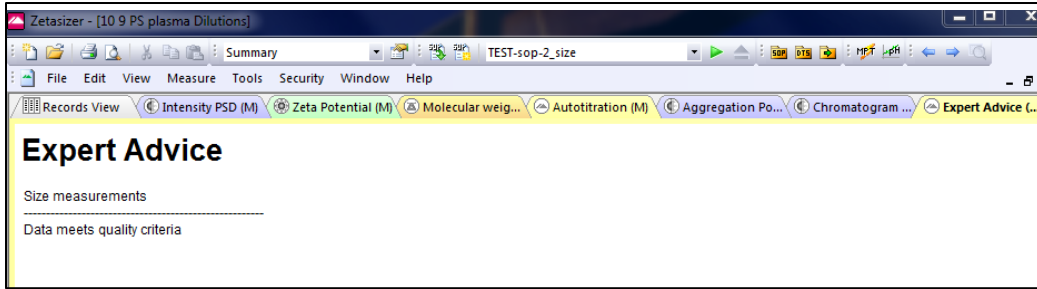


Figure A.13 Description of Data Quality for Dilution 9, Run #3

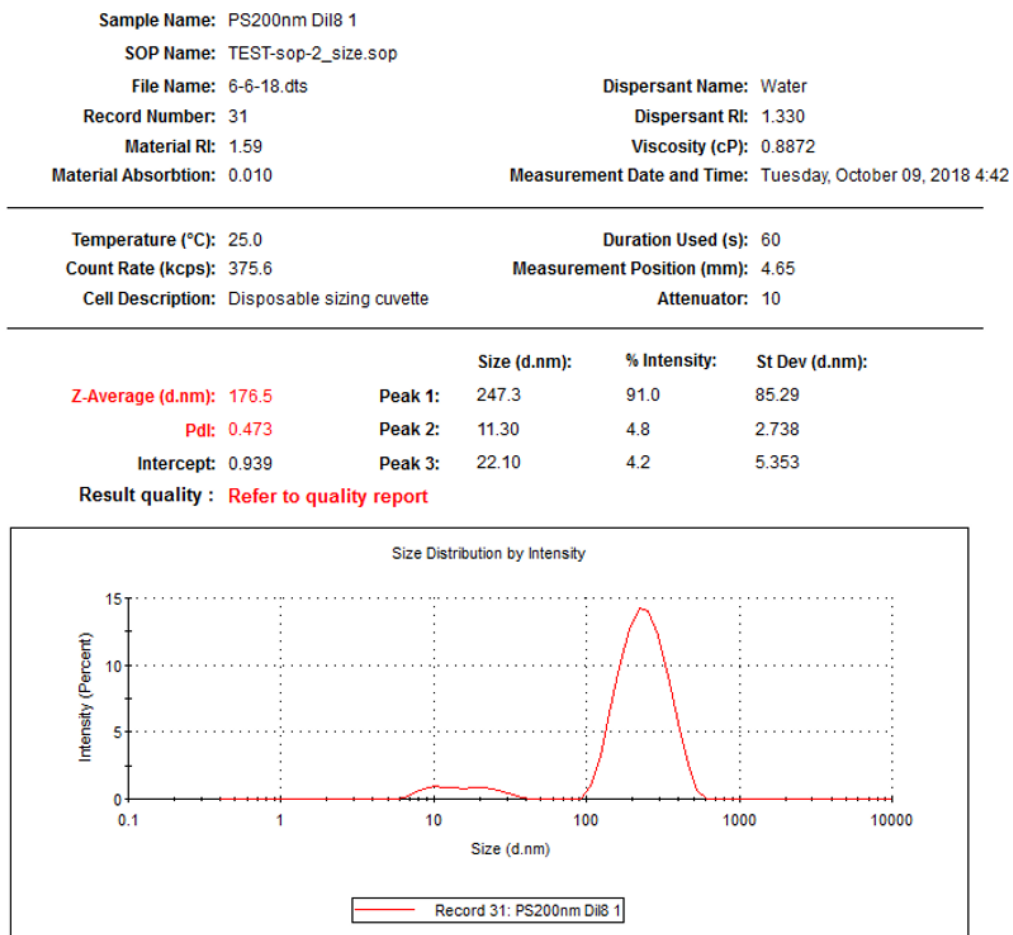


Figure A.14 DLS Results from Polystyrene Nanoparticles Incubated in Dilution 8, Run #1

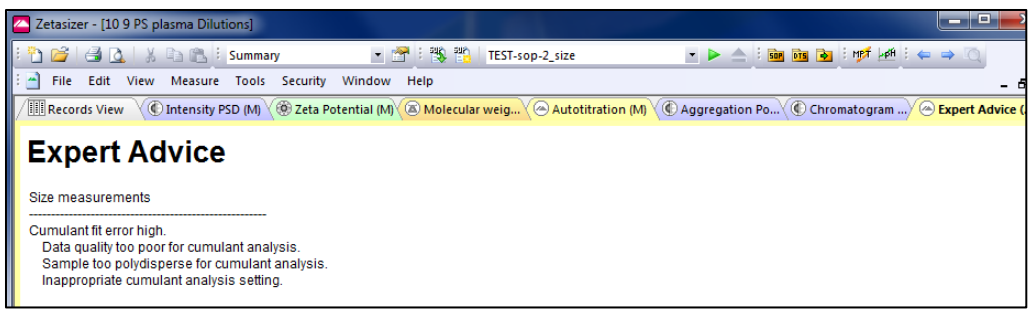


Figure A.15 Description of Data Quality for Dilution 8, Run #1

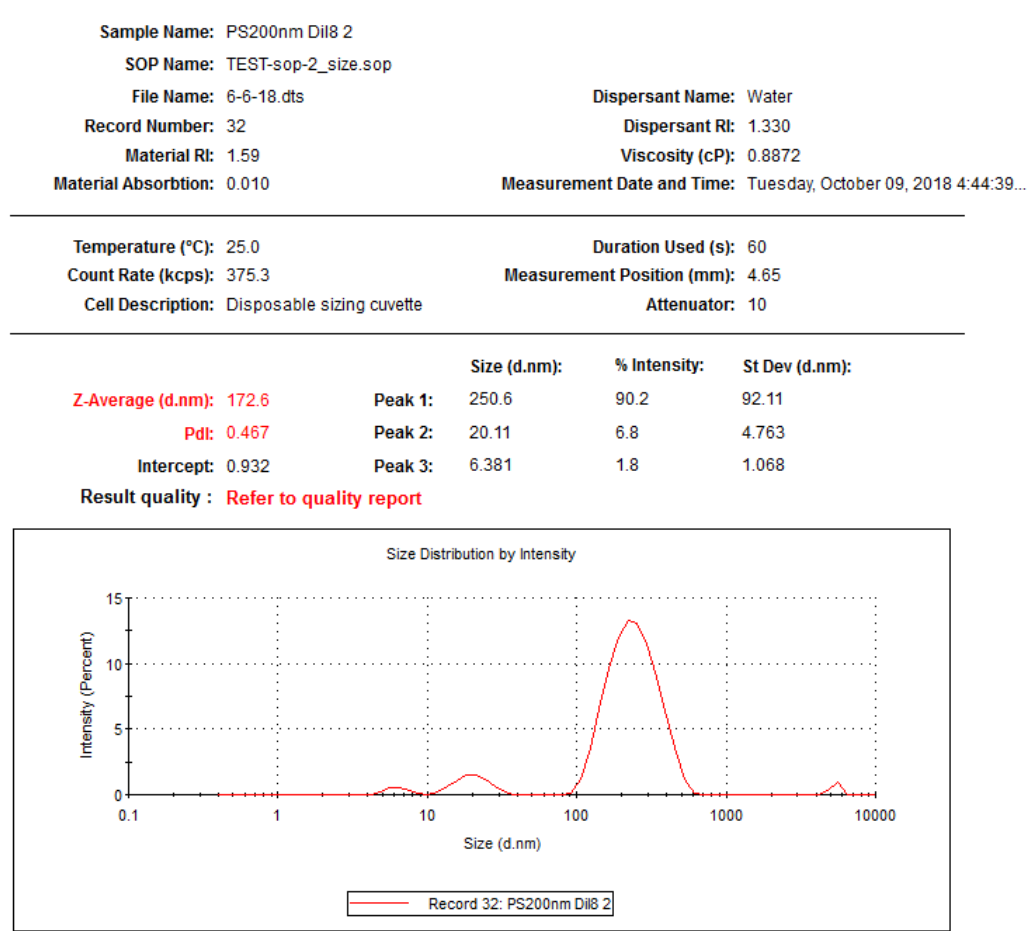


Figure A.16 DLS Results from Polystyrene Nanoparticles Incubated in Dilution 8, Run #2

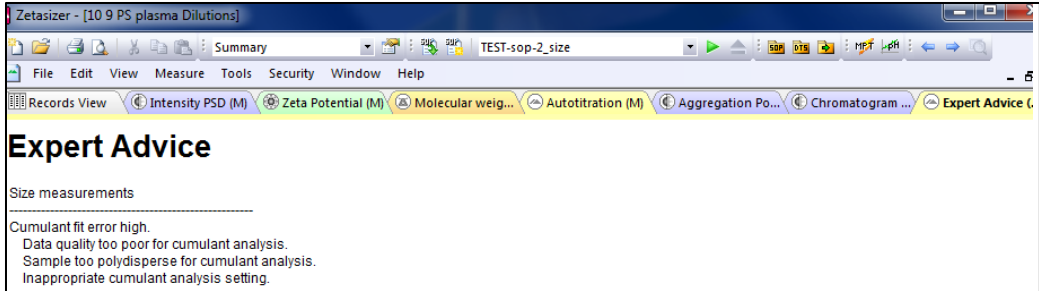


Figure A.17 Description of Data Quality for Dilution 8, Run #2

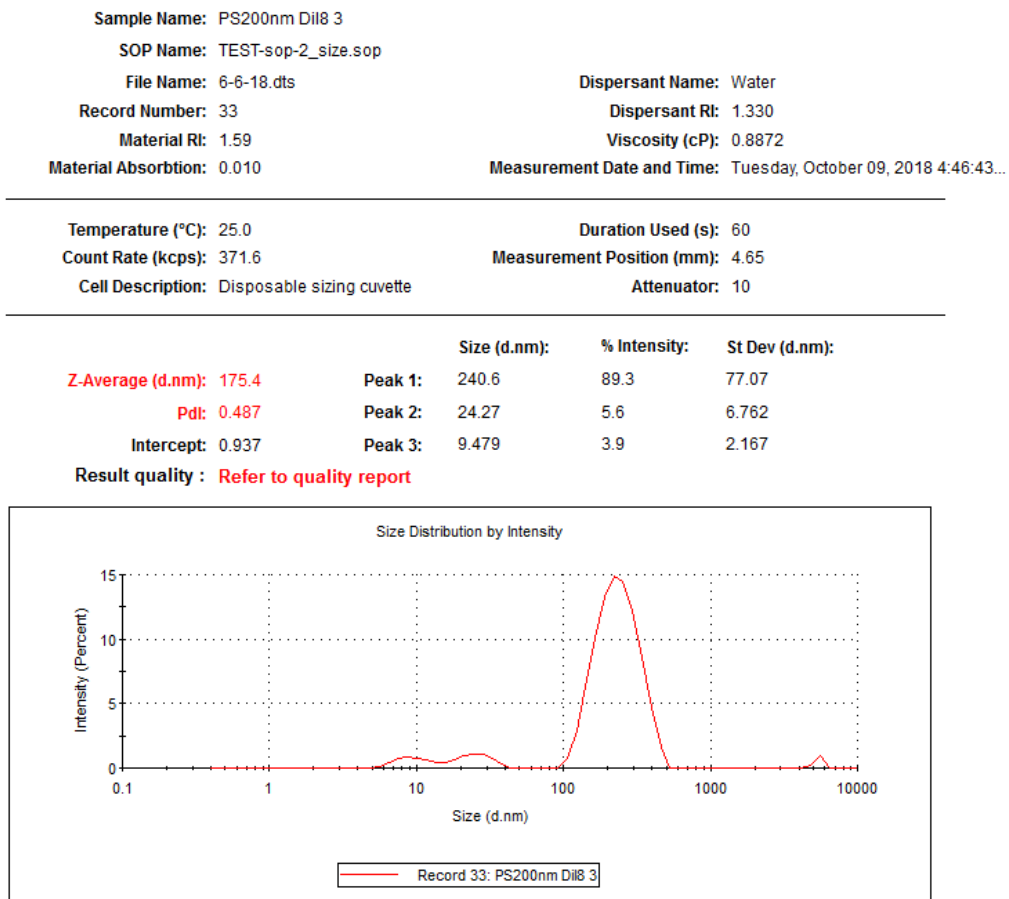


Figure A.18 DLS Results from Polystyrene Nanoparticles Incubated in Dilution 8, Run #3

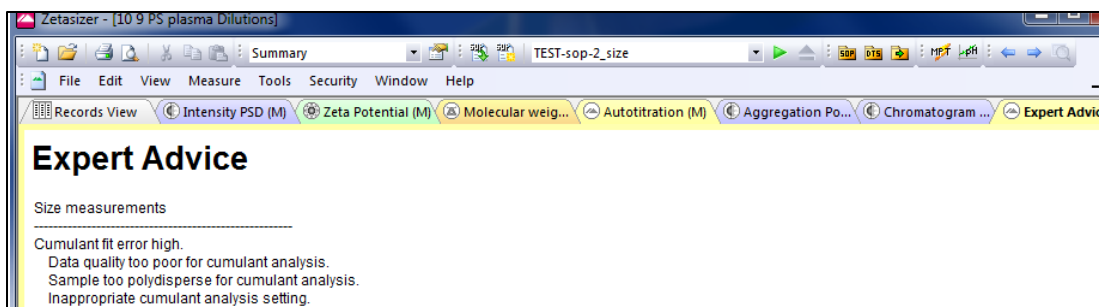


Figure A.19 Description of Data Quality for Dilution 8, Run #3

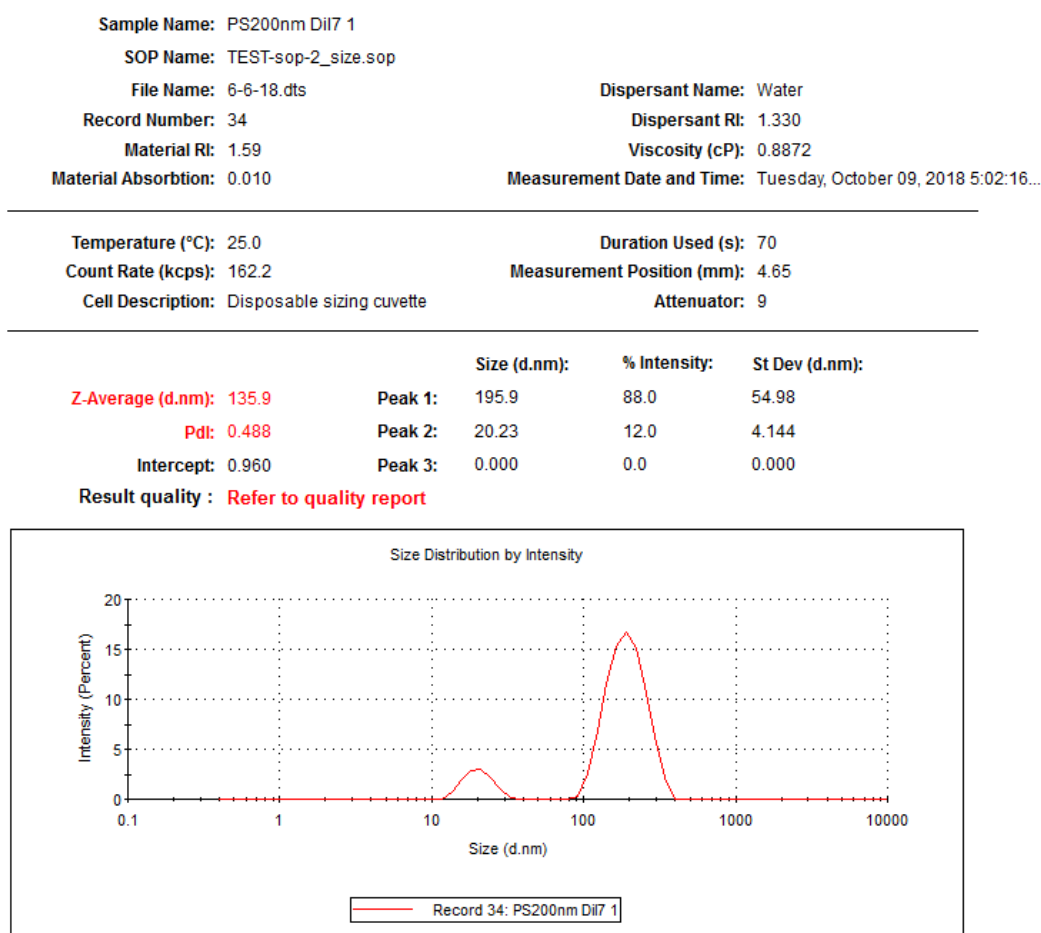


Figure A.20 DLS Results from Polystyrene Nanoparticles Incubated in Dilution 7, Run #1

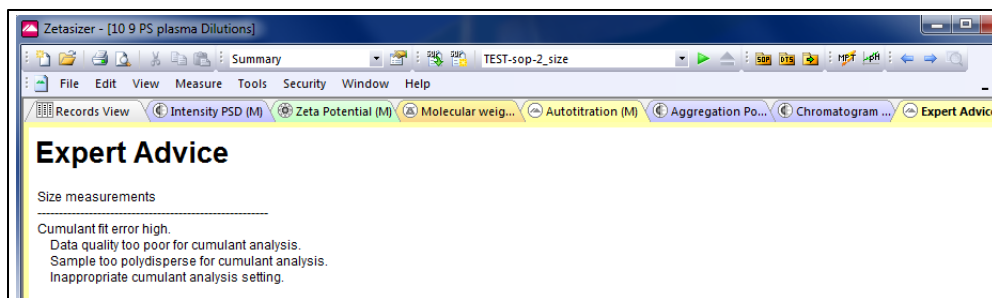


Figure A.21 Description of Data Quality for Dilution 7, Run #1

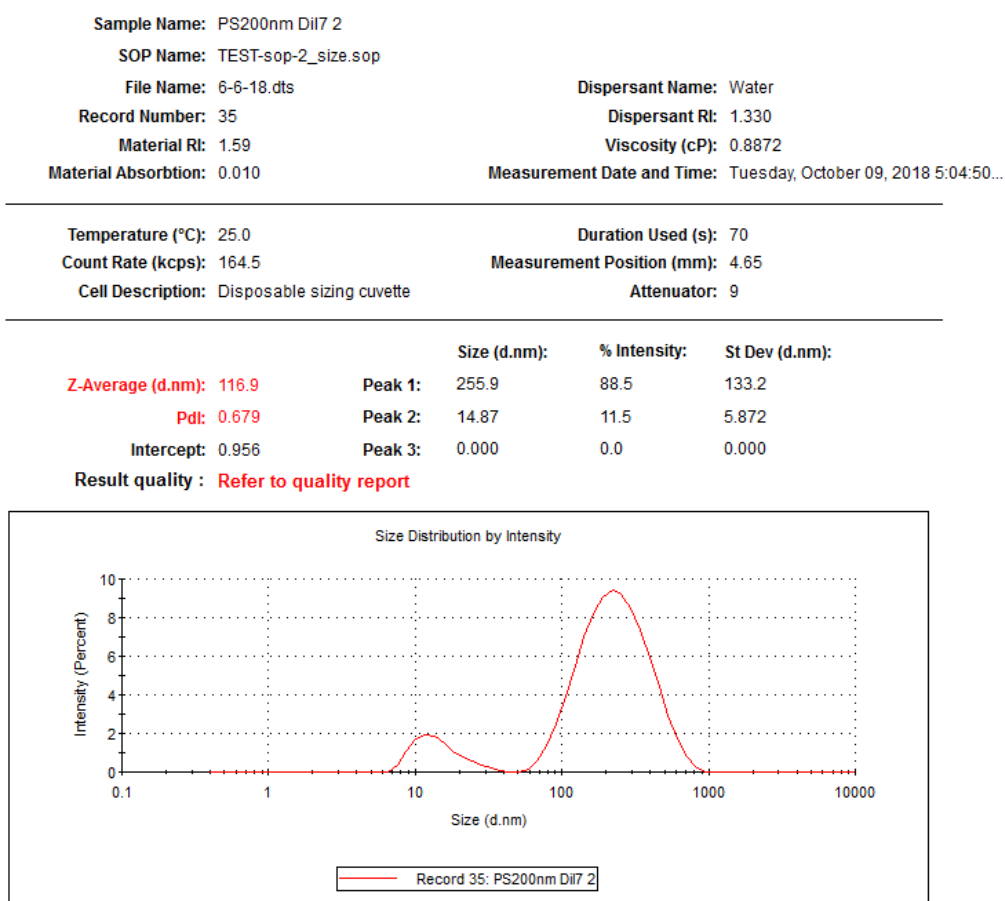


Figure A.22 DLS Results from Polystyrene Nanoparticles Incubated in Dilution 7, Run #2

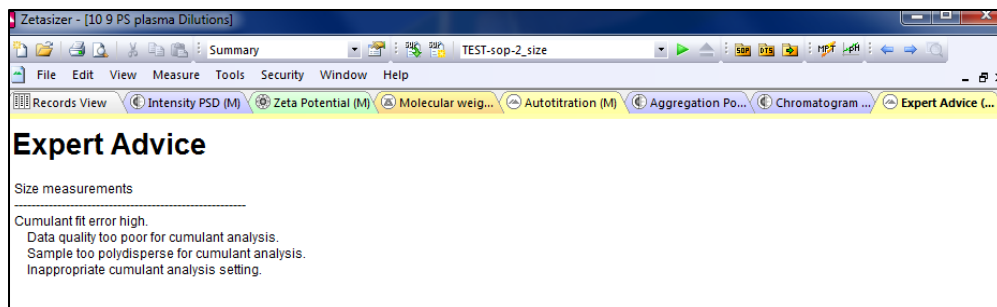


Figure A.23 Description of Data Quality for Dilution 7, Run #2

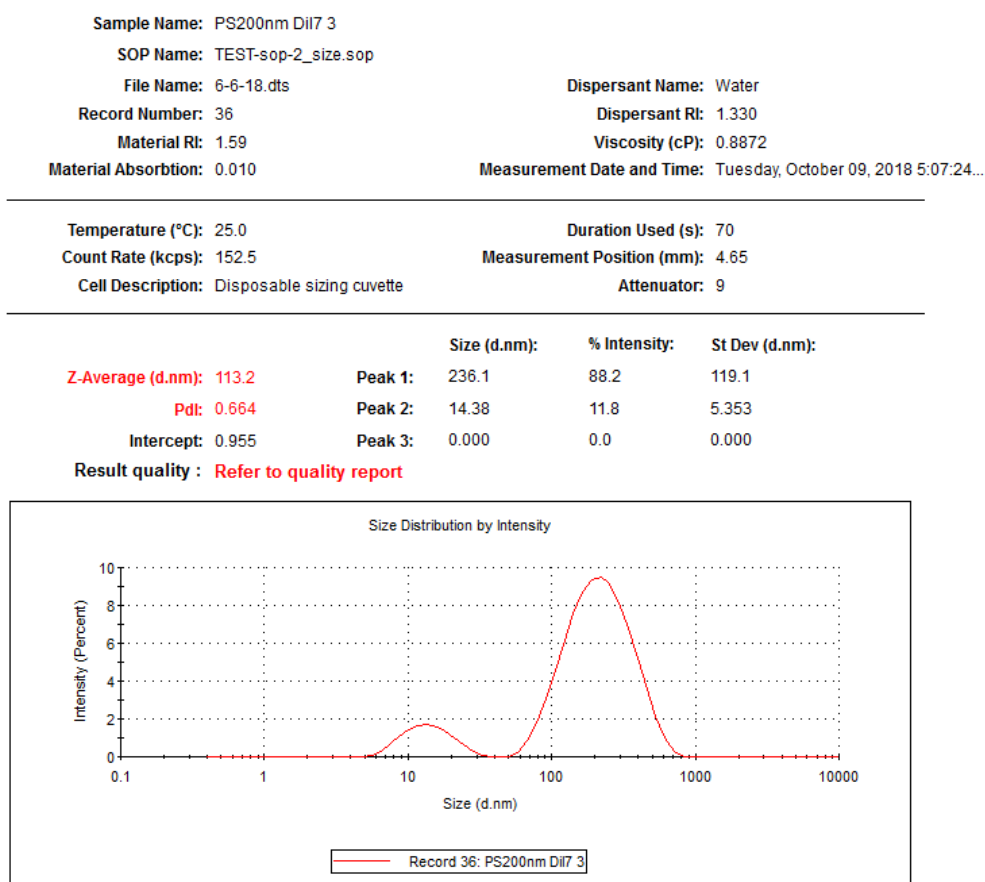


Figure A.24 DLS Results from Polystyrene Nanoparticles Incubated in Dilution 7, Run #3

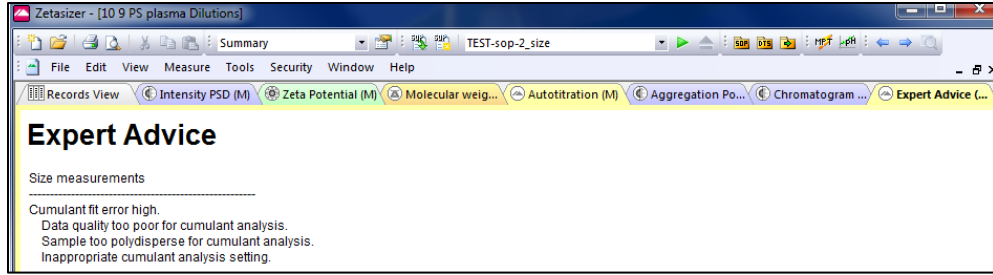


Figure A.25 Description of Data Quality for Dilution 7, Run #3

Sample Name: PS200nm dil6 1	Dispersant Name: Water
SOP Name: TEST-sop-2_size.sop	Dispersant RI: 1.330
File Name: 6-6-18.dts	Viscosity (cP): 0.8872
Record Number: 40	Measurement Date and Time: Tuesday, October 09, 2018 5:33:49...
Material RI: 1.59	
Material Absorption: 0.010	
Temperature (°C): 25.0	Duration Used (s): 70
Count Rate (kcps): 238.4	Measurement Position (mm): 4.65
Cell Description: Disposable sizing cuvette	Attenuator: 9

	Size (d.nm):	% Intensity:	St Dev (d.nm):
Z-Average (d.nm): 75.40	Peak 1: 173.0	79.3	63.69
Pdl: 0.909	Peak 2: 16.24	19.7	7.140
Intercept: 0.954	Peak 3: 5483	1.0	228.4

Result quality : Refer to quality report

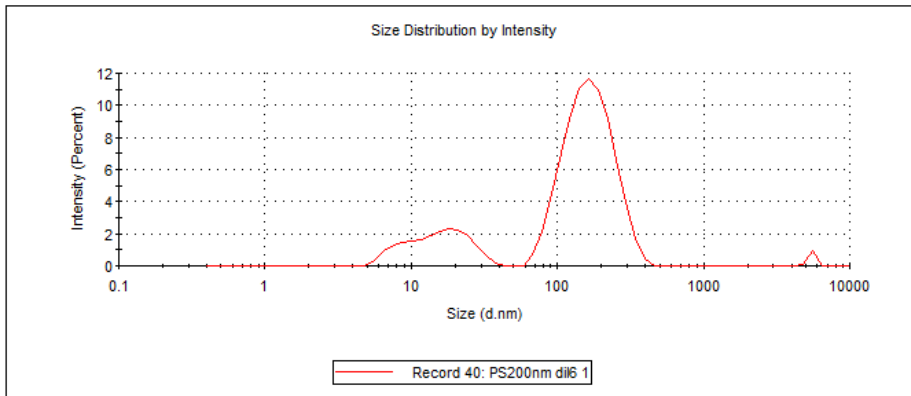


Figure A.26 DLS Results from Polystyrene Nanoparticles Incubated in Dilution 6, Run #1

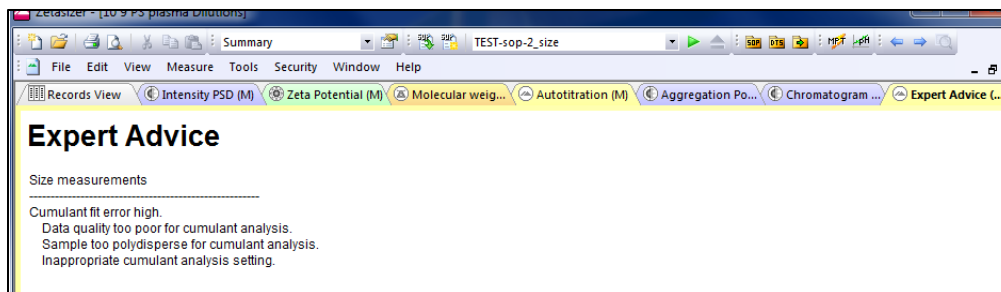


Figure A.27 Description of Data Quality for Dilution 6, Run #1

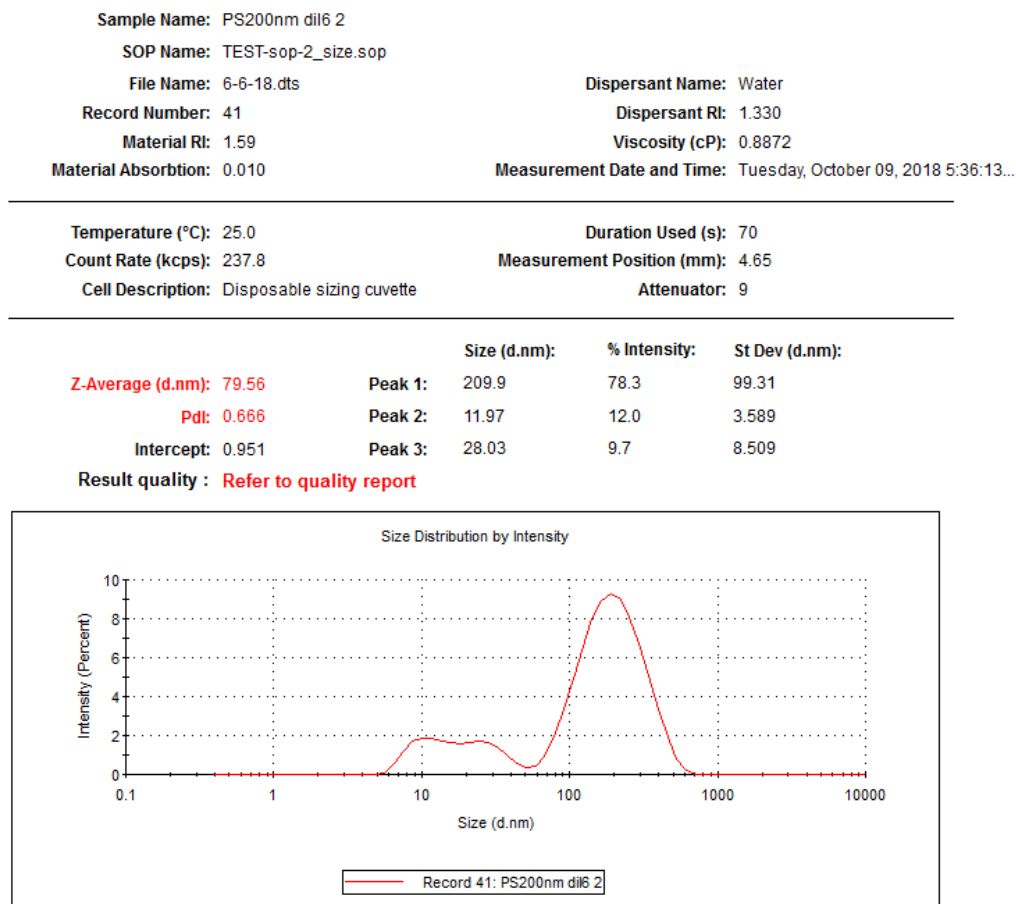


Figure A.28 DLS Results from Polystyrene Nanoparticles Incubated in Dilution 6, Run #2

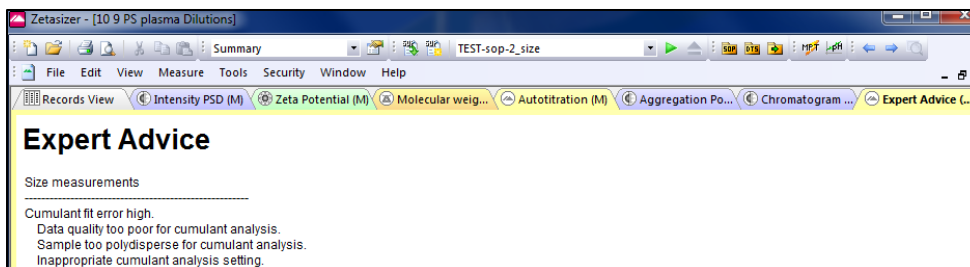


Figure A.29 Description of Data Quality for Dilution 6, Run #2

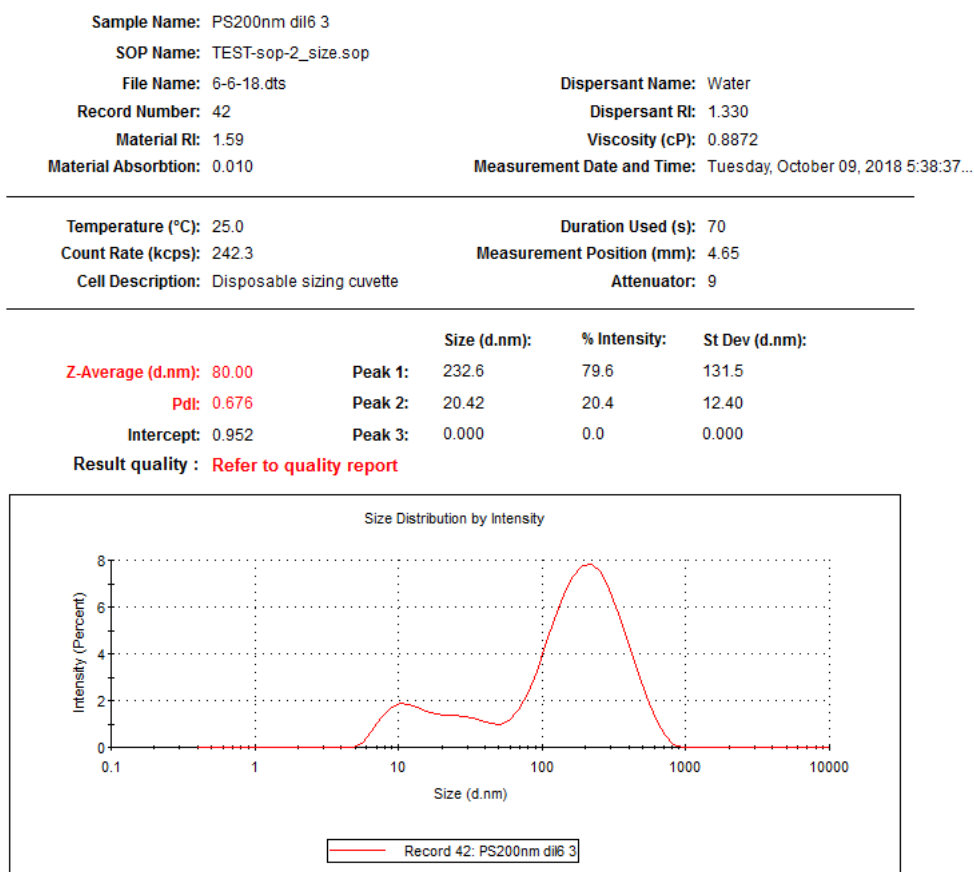


Figure A.30 DLS Results from Polystyrene Nanoparticles Incubated in Dilution 6, Run #3

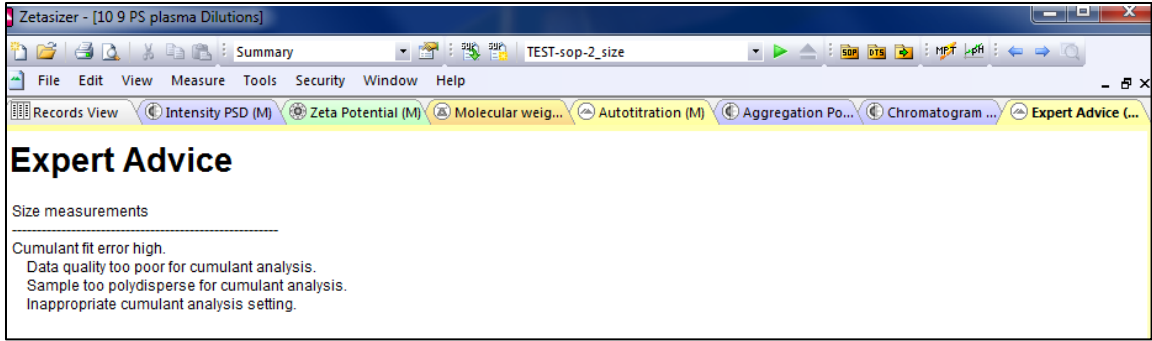


Figure A.31 Description of Data Quality for Dilution 6, Run #3

The individual data shown in Figures A.2 through A.31 is summarized in Table A.1. Averages for each dilution were calculated by averaging the most frequently measured nanoparticle hydrodynamic diameter within each dilution, and then displayed in the fifth column of the table.

Table A.1 Hydrodynamic Diameters of Polystyrene Particles Incubated in Plasma 2 Dilutions Using DLS

Dilution	Run	Peak Size (nm)	% Intensity	Average of Mode	Count	Standard Deviation	Standard Error
6	1	173.00	79.30	205.17	42	8.89	1.37
		16.24	19.70				
		5483.00	1.00				
	2	209.90	78.30				
		11.97	12.00				
		28.03	9.70				
	3	232.60	79.60				
		20.42	20.40				
		-	-				
7	1	195.90	88.00	229.30	42	9.39	1.45
		20.23	12.00				
		-	-				
	2	255.90	88.50				
		14.87	11.50				
		-	-				
	3	236.10	88.20				
		14.38	11.80				
		-	-				
8	1	247.30	91.00	246.17	36	9.50	1.58
		11.30	4.80				
		22.10	4.20				
	2	250.60	90.20				
		20.11	6.80				
		6.38	1.80				
	3	240.60	89.30				
		24.27	5.60				
		9.50	3.90				
9	1	244.70	94.40	262.77	36	9.91	1.65
		14.92	4.90				
		6.95	0.70				
	2	290.40	100.00				
	3	253.20	100.00				
	Saline	1	207.90				
2		233.30	100.00				
3		237.70	100.00				

APPENDIX B

Viscometry

Due to the required accuracy needed for the Nanosight NS300 to correctly distinguish the size of the particles to the nanometer, a Fisherbrand Traceable thermometer was used to closely monitor and ensure that the temperature was retained at 37°C. Fourteen milliliters of each dilution were prepared and heated to 37°C by means of a water bath. These samples were then loaded into a glass Ubbelohde capillary viscometer. Ten separate measurements were taken at 37°C for each dilution. In order to attain the dynamic viscosity of each dilution, the measured kinematic viscosity in $\frac{\text{m}^2}{\text{s}}$ was multiplied by the density of the dilution's density, in $\frac{\text{kg}}{\text{m}^3}$, in order to get the dynamic viscosity, in $\frac{\text{kg}}{\text{m}\times\text{s}}$. The results attained from this method are summarized in Table B.1.

Table B.1 Kinematic Viscosity of Dilutions of Goat Blood Plasma and Saline Converted to Dynamic Viscosity Using Density

Dilution #	Measured Kinematic Viscosity ($\frac{m^2}{s}$)	Density ($\frac{kg}{m^3}$)	Converted Dynamic Viscosity ($\frac{kg}{m \times s}$)	Standard Error ($\frac{kg}{m \times s}$)
Dilution 0	0.970	1	0.970	0.003
Dilution 1	0.841	1	0.841	0.006
Dilution 2	0.769	1	0.769	0.003
Dilution 3	0.747	1	0.747	0.005
Dilution 4	0.732	1	0.732	0.003
Dilution 5	0.727	1	0.727	0.004
Dilution 6	0.722	1	0.722	0.001
Dilution 7	0.736	1	0.736	0.002
Dilution 8	0.730	1	0.730	0.001
Dilution 9	0.738	1	0.738	0.003

To measure the density of each dilution, a 2mL Eppendorf tube was massed and then loaded with either 500, 750, or 1000 μ L of one of the ten dilutions. The overall mass of the tube and the solution would then be taken, and the mass of the tube would be subtracted from the overall mass in order to calculate the final mass of the dilution. The mass of the solution would then be divided by the overall volume in order to achieve the density in final units of $\frac{kg}{m^3}$. This process was repeated for each dilution, and the standard deviation was then taken between the three volumes. The error between the three

measurements was determined small enough to conclude that the amount of volume used to measure did not affect the overall density measurement, and therefore all 30 individual measured densities for each dilution were averaged. There was clearly an error in the values of the measured dilutions, and the averaged values are included in the Table B.2.

Table B.2 Actual Density Values of Each Dilution

Dilution	Average Density ($\frac{\text{kg}}{\text{m}^3}$)	Standard Deviation	Standard Error ($\frac{\text{kg}}{\text{m}^3}$)
Dilution 0	0.990	0.004	0.001
Dilution 1	0.978	0.010	0.003
Dilution 2	0.947	0.023	0.008
Dilution 3	0.973	0.007	0.002
Dilution 4	0.966	0.016	0.005
Dilution 5	0.969	0.004	0.001
Dilution 6	0.977	0.020	0.007
Dilution 7	0.972	0.003	0.001
Dilution 8	0.967	0.009	0.003
Dilution 9	0.971	0.025	0.008

The density of saline solution is $1.0046 \frac{\text{kg}}{\text{m}^3}$, and human blood plasma can be approximated to around $1.0025 \frac{\text{kg}}{\text{m}^3}$ [7] [21]. By this logic, the density of any dilution of blood plasma and saline solution needs to be in between those two values. All the calculated average densities were consistently under $1 \frac{\text{kg}}{\text{m}^3}$, which is obviously not the correct density

of any of the dilutions. This error could have occurred in the actual measurement, although the consistency and low standard error in measurements says otherwise. The most likely source of error comes from clotting factors within the plasma, such as fibrinogen, aggregating within the plasma over time, and affecting the density of the plasma upon measurement, as these measurements were done on Plasma 1 well after the earlier experiments were completed.

Because the densities of the two solutions are so close to $1 \frac{\text{kg}}{\text{m}^3}$, substituting the measured kinematic viscosity as the dynamic viscosity would produce less error than using the measured densities of the blood plasma to convert between the two. As a matter of fact, the error within the Nanosight NS300's individual measurements are larger than the error provided with this substitution. Therefore, in order to correctly measure the hydrodynamic viscosities of the particles in each dilution, the kinematic viscosity was considered equal to the dynamic viscosity of each dilution.

APPENDIX C
NANOPARTICLE TRACKING ANALYSIS

C.1 Malvern Nanosight NS300

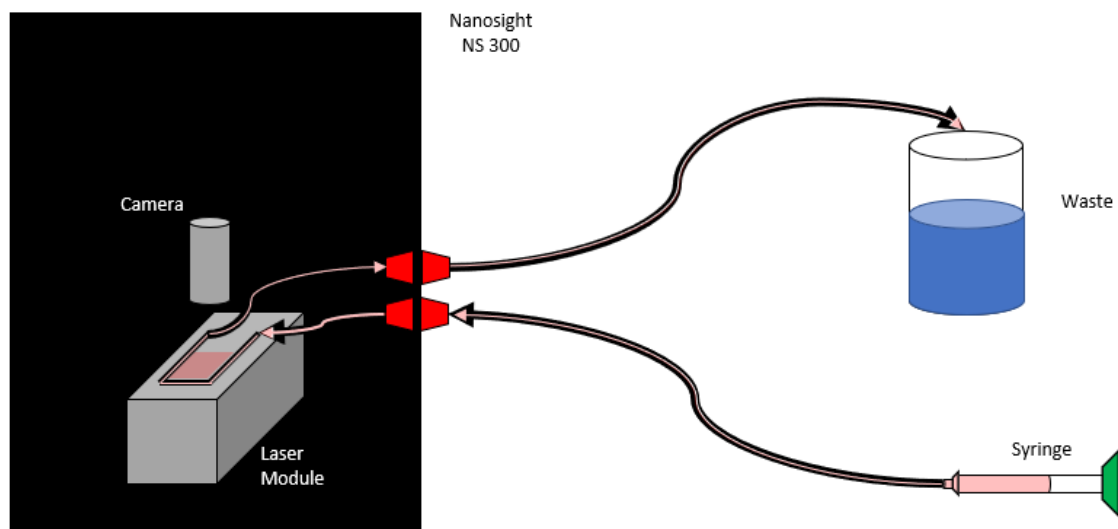


Figure C.1 Schematic of Malvern Nanosight NS300

Figure C.1 displays a schematic of the Nanosight NS300. First, a sample is loaded into a syringe, which is then connected to a tube that feeds into the Nanosight. The sample is then pumped into a microfluidic device sitting on top of a laser module. An objective attached to a camera hangs over this viewing plate and has the ability to record the light scattered by the particles as the laser sends light through the sample. The data captured by the camera is then analyzed, during which each beam of scattered light is analyzed by the Nanosight NS300 to calculate the measured hydrodynamic diameter of each particle. A “mode size” is then reported, which represents the most frequently measured size of the particles in solution.

C.2 Dilution Experiment

The measurement procedure was repeated with two sets of blood plasma and pure saline, and the data is summarized for each run of each dilution in Tables C.1 – C.5.

Table C.1 Hydrodynamic Diameters of Polystyrene Nanoparticles Incubated in Plasma 2

Dilution #	Percent of Plasma in Solution	Average Mode (nm)	Count	Standard Deviation (nm)	Standard Error (nm)
Dilution 0	100	297.98	22	9.63	2.05
Dilution 1	50	303.11	24	7.70	1.57
Dilution 2	25	269.54	24	58.17	11.87
Dilution 3	12.5	283.33	27	11.95	2.30
Dilution 4	6.25	275.32	20	8.57	1.92
Dilution 5	3.125	277.64	30	11.12	2.03
Dilution 6	1.5625	270.91	26	7.35	1.44
Dilution 7	0.78125	263.12	21	4.64	1.01
Dilution 8	0.390625	262.55	23	4.81	1.00
Dilution 9	0.1953125	269.57	26	8.63	1.69

Table C.2 Raw Data Used to Calculate the Hydrodynamic Diameters of Polystyrene Nanoparticles Incubated in Plasma 2

	"Plasma %"	User	Date	Data										Average	Count	Standard Deviation	Standard Error	
Dilution 0	100	Mark	29-Jun	306.77	300.38	303.11	297.87	308.71	296.00		307.85	306.34			300.93	22	9.723703995	2.073100657
		Mark	29-Jun	288.54	303.26	295.86	287.67	289.04	302.40	297.59								
		Alison	6-Jul	318.48	317.62	314.53	292.40	309.28	284.36	292.48								
Dilution 1	50	Mark	29-Jun	312.27	307.07	312.52	306.39	308.58	300.52	302.79					309.85	24	7.87345059	1.607161372
		Alison	29-Jun	302.87	313.27	311.26	329.80	310.34	299.26	303.54	306.56	299.18	304.21					
Dilution 2	25	Alison	30-Jul	324.78	316.48	304.65	316.31	320.08	307.50	316.14					296.96	23	10.1419344	2.114739508
		Karen	26-Jun	291.37	289.38	290.80	289.19	286.92	281.80	279.62	282.84	282.18						
		Alison	29-Jun	298.13	298.42	298.99	305.53	300.88	304.49	298.70	301.74							
Dilution 3	12.5	Alison	29-Jun	307.96	300.57	312.60	311.75	309.10	307.11					291.30	27	12.28498347	2.364246171	
		Alison	29-Jun	280.30	281.34	283.15	277.74	280.96	272.70	281.34	274.70	272.51	270.23					
		Mark	2-Jul	295.97	292.84	288.28	300.15	296.16	297.87	296.45	292.37	293.98	293.98					
Dilution 4	6.25	Alison	30-Jul	310.10	306.50	303.36	300.32	303.55	311.34	306.97				284.91	20	8.868639773	1.98308814	
		Mark	30-May				255.78					271.86						
		Mark	2-Jul	301.92	284.36	288.46	286.90	289.82	288.56	283.68								
Dilution 5	3.125	Mark	2-Jul	290.59	286.29	287.76	280.44	286.00	287.27	283.47	285.71	291.66	286.20	286.62	30	11.47889777	2.095750415	
		Alison	3-Jul	303.51	299.69	304.19	298.91	303.02	297.44	294.11	300.38	292.15	292.15					
		Alison	3-Jul	297.55	287.27	292.07	296.77	288.54	282.18	287.17	278.55	284.53	277.67					
Dilution 6	1.5625	Mark	10-Jul	273.98	275.16	277.31	274.96	270.26	282.31	276.62	273.88	263.69	272.51	284.95	26	7.72615965	1.51522457	
		Alison	3-Jul	288.02	288.41	287.14	284.01	284.79	278.24	280.98	284.10	282.54	286.16					
		Mark	16-Jul	309.11	291.22	294.35	291.02	290.14	287.21	281.34	282.51	280.36						
Dilution 7	0.78125	Alison	30-Jul	289.59	280.40	286.26	283.92	275.90	266.61	274.33				270.67	21	4.771497525	1.041226123	
		Karen	3-Jul	269.98	266.70	264.68	264.87	267.86	267.09	266.51								
		Karen	3-Jul	275.95	272.67	272.09	277.87	271.61	280.57	275.37								
Dilution 8	0.390625	Karen	3-Jul	277.68	268.33	272.67	272.47	268.43	265.44	265.15				272.99	23	5.000497393	1.042675784	
		Miriam	3-Jul	272.20	273.27	267.90	272.98	272.78	266.04	262.42								
		Miriam	3-Jul	270.10	277.24	273.43	271.67	273.43	270.30	266.97								
Dilution 9	0.1953125	Alison	10-Jul	281.19	281.19	276.39	280.99	270.24	280.70	275.12	272.19	269.94		272.29	26	8.628454371	1.692179123	
		Miriam	5-Jul			272.05	267.79	268.27	265.24	267.32	264.11	266.37	262.03					277.40
		Alison	13-Jul	271.37	288.58	279.60	267.59		263.53	258.05	261.83							
		Mark	16-Jul	291.24	290.01	277.25	274.22	274.98	275.83	271.96	280.18	270.63	272.14					

Table C.3 Hydrodynamic Diameters of Polystyrene Particles Incubated in Plasma 1

Dilution #	Percent of Plasma in Solution	Average Mode (nm)	Count	Standard Deviation (nm)	Standard Error (nm)
Dilution 0	100	294.73	42	21.78	3.36
Dilution 1	50	286.74	42	32.33	4.99
Dilution 2	25	284.34	35	21.41	3.62
Dilution 3	12.5	272.04	28	8.28	1.56
Dilution 4	6.25	272.23	25	12.76	2.55
Dilution 5	3.125	263.35	28	15.92	3.01
Dilution 6	1.5625	266.35	49	11.30	1.61
Dilution 7	0.78125	253.75	30	7.18	1.31
Dilution 8	0.390625	253.32	29	7.71	4.32
Dilution 9	0.1953125	251.74	28	9.83	1.86

Table C.4 Hydrodynamic Diameters of Polystyrene Particles Incubated in Saline Solution

Dilution #	Percent of “Plasma” in Solution	Average Mode (nm)	Count	Standard Deviation (nm)	Standard Error (nm)
Dilution 0	100	204.45	25	24.34	4.87
Dilution 1	50	203.04	30	7.59	1.39
Dilution 2	25	202.69	25	8.52	1.70
Dilution 3	12.5	205.79	30	8.02	1.47
Dilution 4	6.25	200.01	30	6.82	1.25
Dilution 5	3.125	207.86	25	12.34	2.47
Dilution 6	1.5625	200.49	30	5.83	1.06
Dilution 7	0.78125	204.51	27	18.96	3.65
Dilution 8	0.390625	203.01	28	8.76	1.66
Dilution 9	0.1953125	201.92	30	5.33	0.97

Table C.5 Raw Data Used to Calculate Hydrodynamic Diameters of Polystyrene Particles Incubated in Saline Solution

	"Plasma %"	Date												Average	Count	Standard Deviation	Standard Error
Dilution 0	100	22-May	192.1	213.3	207.4	220.8	157.5	180.3	221	135				204.448	25	24.34145715	4.868291429
		6-Jul	213.4	212.4	219.4	218.8	218.1	225.6	214.5	215	219.3	211.9					
		8-Jun	195.2	188.9		179.5	231.2	207.7		184.1		228.8					
Dilution 1	50	19-Jul	198.1	197.3	196.9	197.1	197	192.1	198.3	197.2	194	196.5	203.0366667	30	7.587352604	1.385254724	
		17-Jul	207.3	212.2	203.3	196.4	214	205.2	213.9	205.6	194.7	222.8					
			204.7	199.4	207.4	198.7	206.9	202.9	205.9	200.7	205.5	219.1					
Dilution 2	25	22-May		189		219.1	197.3	187				220.9	202.696	25	8.523031542	1.704606308	
		11-Jul	205.2	203.3	206.5	202.7	202.8	202.2	206.3	202.9	209.7	205					
			199.6	193	200.5	200.5	200.4	213.4	199.8	211.1	203.2	186					
Dilution 3	12.5	18-Jul	211.8	215.1	216.6	216.2	216.3	216	207.8	212	219.6	218.7	205.7933333	30	8.024485517	1.46506391	
		11-Jul	202.7	200.9	196.2	193.6	202.1	202.2	200.9	198.6	202.9	197.7					
		12-Jul	199.1	198.7	207.2	203.1	210	189.5	210.4	202.6	205.5	199.8					
Dilution 4	6.25	12-Jul	193.7	218.4	206.5	198.8	217.7	198.5	202.3	206.3	201.1	206.9	200.0133333	30	6.821403098	1.245412117	
			190.8	195.5	204.3	195.7	196.7	198	194.3	190	196.6	196.2					
			199.6	202.3	206.3	194.1	202	195.9	202.8	200.8	190.6	197.7					
Dilution 5	3.125	22-May	201.9	204.9	208.3	202	200.6	201.5	195.9	202.7	190.4	197.4	207.856	25	12.33916799	2.467833598	
		12-Jun	196	250.4	195	205.4		200.4									
		18-Jul	214	204.1	206.4	220.1	217.4	213.9	211.7	222.7	216.5	216.8					
Dilution 6	1.5625	13-Jul	195.3	188.3	201.3	196.5	192.7	202.6	195.1	190.5	217.3	196.7	200.4866667	30	5.829812402	1.064373253	
			198.7	199.6	201.4	202.2	211.6	204.3	198.8	199.6	196.2	200.4					
		18-Jul	202.9	198.8	201.2	207.2	199	201.5	200.3	204.7	201.8	208.1					
Dilution 7	0.78125	13-Jul	202.9	205.6	205.3	203.9	204.5	204.3	200	198.7	199.5	203.8	204.5074074	27	18.95518857	3.647927741	
		26-Jun		217.9	229.9	223	221.7	220.4	222.5		243.1	243.8					
		26-Jun		182.2	181.3	187.7	188.9	186.8	169.1	209.4	176.2	189.3					
Dilution 8	0.390625	13-Jul	201.6	198.9	197.9	199.8	196.9	201.5	195.7	202.3	202.1	201.2	203.0107143	28	8.762095948	1.655880489	
			192.4	193.5	193	194.5	193.2	197.7	198	203	193.2	206.8					
		26-Jun	218.2	216.8	213.4	216.6	220.7	208.2			215.4	211.8					
Dilution 9	0.1953125	19-Jul	197.4	198.2	203.9	200.6	193	201.4	192.9	196.4	202.5	195.9	201.9166667	30	5.328652759	0.9728744391	
		16-Jul	199	201.6	202.1	210.4	202.8	209.2	199.8	210.8	201.3	205.8					
		17-Jul	202.1	204.4	197.6	210.6	204	198.7	201.8	214	194.6	204.7					

Table C.6 Fitted Equations Relating Hydrodynamic Diameter with Percentage of Plasma in Dilution

Data Set	Equation	R ²
Plasma 2	$Y = 14.21 \times \log_{10}(X) + 276.41$	0.79
Plasma 1	$Y = 14.89 \times \log_{10}(X) + 265.82$	0.90
Saline	$Y = 0.58 \times \log_{10}(X) + 202.35$	0.06

Tables C.7 and C.8 display the measured protein corona thickness in each dilution.

The calculations to produce these values are discussed in length in Chapter 4.

Table C.7 Average Protein Corona Thickness of Polystyrene Particles Incubated in Plasma
1

Dilution	Average Corona Thickness	Standard Deviation	Standard Error	Percent Change	Standard Error
Dilution 0	45.14	25.12	3.02	22.08%	0.07
Dilution 1	41.85	33.12	4.21	20.61%	0.08
Dilution 2	40.82	23.04	2.97	20.14%	0.06
Dilution 3	33.13	11.53	1.51	16.10%	0.04
Dilution 4	36.11	15.07	2.03	18.05%	0.04
Dilution 5	28.03	17.32	2.38	13.49%	0.07
Dilution 6	32.93	16.73	1.88	16.43%	0.04
Dilution 7	24.62	9.250	1.23	12.04%	0.08
Dilution 8	25.15	20.46	2.71	12.39%	0.04
Dilution 9	23.99	13.17	1.90	11.77%	0.04

Table C.8 Average Protein Corona Thickness of Polystyrene Particles Incubated in Plasma
2

Dilution	Average Corona Thickness	Standard Deviation	Standard Error	Percent Change	Standard Error
Dilution 0	48.24	4.86	1.04	23.60%	0.09
Dilution 1	53.41	3.94	0.8	26.31%	0.03
Dilution 2	47.13	5.07	1.06	23.25%	0.04
Dilution 3	42.76	6.14	1.18	20.78%	0.04
Dilution 4	42.45	4.43	0.99	21.22%	0.03
Dilution 5	39.38	5.74	1.05	18.95%	0.05
Dilution 6	42.23	3.86	0.76	21.06%	0.03
Dilution 7	33.08	2.39	0.52	16.18%	0.07
Dilution 8	34.99	2.5	0.52	17.24%	0.04
Dilution 9	35.19	4.31	0.85	17.43%	0.03

REFERENCES

1. Anisha A. D'souza & Ranjita Shegokar (2016) Polyethylene glycol (PEG): a versatile polymer for pharmaceutical applications, *Expert Opinion on Drug Delivery*, 13:9, 1257-1275, DOI: [10.1080/17425247.2016.1182485](https://doi.org/10.1080/17425247.2016.1182485)
2. Armenante, Piero. "Transport Through Biological Barriers." *PhEn 618: Pharmacokinetics and Drug Delivery*. PhEn 618: Pharmacokinetics and Drug Delivery, 19 Feb. 2018, Newark, New Jersey, The New Jersey Institute of Technology.
3. "Blood." *Blood - The Human Heart: An Online Exploration from The Franklin Institute, Made Possible by Unisys*, The Franklin Institute.
4. "Brownian Motion." *Merriam-Webster*, Merriam-Webster
5. Busher JT. Serum Albumin and Globulin. In: Walker HK, Hall WD, Hurst JW, editors. *Clinical Methods: The History, Physical, and Laboratory Examinations*. 3rd edition. Boston: Butterworths; 1990. Chapter 101.
6. "Dynamic Light Scattering: An Introduction in 30 Minutes." Malvern Instruments Ltd.
7. Fluid Density Calculator Archived 2009-09-16 at the Wayback Machine. earthwardconsulting.com. Retrieved on 2011-02-27.
8. Fournier, Basic Transport Phenomena in Biomedical Engineering, 1999, p. 5.
9. Ghosh, Partha, et al. "Gold Nanoparticles in Delivery Applications." *Advanced Drug Delivery Reviews*, Elsevier, 10 Apr. 2008
10. Goldberg, W. I. "Dynamic Light Scattering." *American Journal of Physics*, vol. - 67, no. 12, July 1999, pp. 1152–1160., doi:10.1119/1.19101.
11. Kim, Hae-Young. "Analysis of Variance (ANOVA) Comparing Means of More than Two Groups." *Restorative Dentistry & Endodontics* 39.1 (2014): 74 - 77. *PMC*. Web. 13 Oct. 2018.
12. Lavrakas, Paul J. "Interaction Effect." *Encyclopedia of Survey Research Methods*, Sage, 2008.

13. M. Rahman et al., Protein-Nanoparticle Interactions, Springer Series in Biophysics, 15, doi:10.1007/978-3-642-37555-2_2, © Springer-Verlag Berlin Heidelberg 2013
14. Malvern Instruments Ltd. *Nanosight Range: Visualize and Measure Nanoparticle Size and Concentration*, Malvern Instruments Ltd., 2016.
15. Mirshafiee, Vahid, et al. “The Importance of Selecting a Proper Biological Milieu for Protein Corona Analysis in Vitro: Human Plasma versus Human Serum.” *The International Journal of Biochemistry & Cell Biology*, vol. 75, June 2016, pp. 188–195., doi:10.1016/j.biocel.2015.11.019.
16. Morris, Bede, and F. C. Courtice. “The Protein And Lipid Composition Of The Plasma Of Different Animal Species Determined By Zone Electrophoresis And Chemical Analysis.” *Quarterly Journal of Experimental Physiology and Cognate Medical Sciences*, vol. 40, no. 2, 7 Nov. 1955, pp. 127–137., doi:10.1113/expphysiol.1955.sp001104.
17. Ng, Cheng Teng, et al. “Clathrin-Mediated Endocytosis of Gold Nanoparticles in Vitro.” *The Anatomical Record*, vol. 298, no. 2, 2014, pp. 418-427. *Wiley Online Library*, doi:10.1002/ar.23051.
18. Ogee, Agnes, et al. “How to Compare Regression Slopes.” *The Minitab Blog*, Minitab, 13 Jan. 2016, blog.minitab.com/blog/adventures-in-statistics-2/how-to-compare-regression-lines-between-different-models.
19. Pearson, Ryan M., et al. “Biomolecular Corona on Nanoparticles: a Survey of Recent Literature and Its Implications in Targeted Drug Delivery.” *Frontiers in Chemistry*, vol. 2, 27 Nov. 2014, doi:10.3389/fchem.2014.00108.
20. “Significance of Alsever's Solution.” *Lorne Laboratories Ltd*, Lorne Laboratories Ltd, 7 Mar. 2017
21. The Physics Factbook – Density of Blood
22. Wade Hedegard, *Anatomy & Physiology: Fluids and Transport*. OpenStax CNX. - Jun 27, 2017
23. Weiss, Alessia C. G., et al. “Microfluidic Examination of the ‘Hard’ Biomolecular Corona Formed on Engineered Particles in Different Biological Milieu.” *Biomacromolecules*, vol. 19, no. 7, 18 Apr. 2018, pp. 2580–2594., doi:10.1021/acs.biomac.8b00196.

24. Wilczynski, Cory. "Fibrinogen ." Edited by Eric B Staros, *Fibrinogen: Reference Range, Interpretation, Collection and Panels*, Medscape, 7 Jan. 2017.
25. Zhang, Xiaoning, et al. "Probing the Binding Affinity of Plasma Proteins Adsorbed on Au Nanoparticles." *Nanoscale*, vol. 9, no. 14, 7 Mar. 2017, pp. 4787–4792., doi:10.1039/c7nr01523b